Published in final edited form as:

Nat Neurosci. 2022 January ; 25(1): 61–71. doi:10.1038/s41593-021-00984-5.

Hypothalamic melanin-concentrating hormone regulates hippocampus-dorsolateral septum activity

Jing-Jing Liu[1,2,3], **Richard W. Tsien**[3], **Zhiping P. Pang**[1,2]

[1]Child Health Institute of New Jersey, Rutgers University Robert Wood Johnson Medical School, 89 French Street, New Brunswick, NJ 08901, USA

[2]Department of Neuroscience and Cell Biology, Rutgers University Robert Wood Johnson Medical School, 89 French Street, New Brunswick, NJ 08901, USA

[3]NYU Neuroscience Institute, New York University School of Medicine, New York, NY 10016, USA.

Abstract

Hypothalamic melanin-concentrating hormone (MCH) polypeptide contributes to regulating energy homeostasis, sleep, and memory, though the mechanistic bases of its effects are unknown. Here, in mice, we uncover the physiological mechanism underlying the functional role of MCH signaling in projections to the dorsolateral septum (dLS), a region involved in routing hippocampal firing rhythms and encoding spatial memory based on such rhythms. Firing activity within the dLS in response to dorsal CA3 (dCA3) excitation is limited by strong feed-forward inhibition (FFI). We find that MCH synchronizes dLS neuronal firing with its dCA3 inputs by enhancing GABA release, which subsequently reduces the FFI and augments dCA3 excitatory input strength, both via presynaptic mechanisms. At the functional level, our data reveal a role for MCH signaling in the dLS in facilitating spatial memory. These findings support a model in which peptidergic signaling within the dLS modulates dorsal hippocampal output and supports memory encoding.

Introduction

While information in the brain is largely conveyed by the fast neurotransmitters glutamate and γ-aminobutyric acid (GABA), synaptic communication and complex behavior are further regulated by slower-acting neuromodulators such as neuropeptides[1]. These enlarge the repertoire of regulatory mechanisms that operate on various timescales to control circuit dynamics and behavioral flexibility and robustness[2, 3]. Despite a growing appreciation for the importance of signaling from peptide-containing neurons, there is only a limited

Correspondence: Zhiping P. Pang, zhiping.pang@rutgers.edu.

Contributions

J.J. Liu and Z.P. Pang conceived the study. J.J. Liu performed the experiments and analyzed the data. R.W. Tsien provided constructive intellectual input to the overall study. All authors contributed to the final manuscript.

Competing interests

The authors declare no competing interests.

understanding of how such neurons control information transfer within neural circuits controlling specific behaviors.

An example of this issue is melanin-concentrating hormone (MCH)-expressing neurons, which are located in the lateral hypothalamic area (LHA) and zona incerta[4], and project widely throughout the brain[5–7]. MCH is a polypeptide that has important roles in the mammalian brain, including the control of energy homeostasis[4], sleep[8, 9], learning and memory[10], and social interactions[11]. Studies of activating, inhibiting, or ablating MCH neurons have uncovered pivotal roles in metabolism[12], reward[13], foraging behavior[14], novel object memorization[15], and sleep[8, 9]. MCH neurons also express other neuropeptides like nesfatin[16] or cocaine-amphetamine-regulated transcript (CART)[17], and can release glutamate[18] or GABA[8]. The MCH-dependent and -independent roles of MCH neurons[12, 19–24] are unclear, making it difficult to describe specific impacts on neuronal activity, circuit dynamics, or behavior.

Hypothalamic MCH neurons project to the dorsal lateral septum (dLS), which functions as an integrative relay downstream of the hippocampus (HP)[25, 26]. A key feature of this circuit is CA3 pyramidal neurons of the dorsal hippocampus (dHP), which include place cells encoding spatial features of the environment[25–28]. The dLS in turn projects to the LHA[25, 26] (which governs motivated behaviors) and other brain regions. Indeed, the dLS receives denser innervation from hypothalamic MCH neurons[5, 6, 18, 25, 26] than other brain regions. Furthermore, *in vivo* recordings in freely moving mice show that a significant subgroup of MCH neurons fire action potentials (10~40 Hz) specifically during exploratory behavior[29–31], which also involves place cell activity. This work raises the intriguing possibility that hypothalamic MCH neurons and HP place cells are concurrently active during spatial exploration. However, major questions remain about the mechanisms by which MCH neurons, and possibly MCH itself, shape information transfer in the hippocampo-septal circuit.

In this study, we clarified how the release of MCH *per se* choreographs information transfer in the dLS, thus improving HP-dependent spatial navigation. Using a combination of genetics-aided neural tracing, synaptic physiology, and behavioral testing, we found that MCH peptide exerts multipronged effects on dLS signaling: suppressing spontaneous firing in dLS neurons (i.e., lowering background ‘noise’), presynaptically enhancing dCA3-to-dLS excitatory strength (i.e., increasing input sensitivity), and dampening $GABA_BR$-mediated feed-forward inhibition (i.e., freeing up dLS firing). These distinct yet synergistic actions enable dLS neurons to fire more rapidly in response to high-frequency dCA3 input, which happens in parallel with MCH-induced improvements in spatial learning and memory. Our findings provide an appealing explanation of how peptidergic input to the dLS modulates the processing of dHP output, making it sensitive to behavioral status. The convergence of classical neurotransmission and peptidergic modulation in dLS could render spatial exploratory behavior sensitive to energy state or environmental/social threats[4, 8–11].

Results

MCH reduces the spontaneous activity of dLS-to-LHA neurons

To allow optogenetic manipulation of MCH neuronal activity, AAV-DIO-Channelrhodopsin 2 (ChR2)-eYFP was injected into the LHA of MCH-Cre mice[32]. Additionally, to identify the dLS neurons that project to the LHA (Fig. 1a), microfluorescent RetroBeads were injected into the LHA of the same animal. Optogenetic stimulation in the hypothalamus reliably activated virus-infected neurons at up to 20 Hz (Fig. 1b,c), which is within the physiological firing spectrum of MCH neurons *in vivo* during exploratory behaviors (10~40 Hz)[29–31]. MCH neurons project widely across the brain[6], with dense, varicose-like projections targeting the dLS (Fig. 1d,e). Consistent with a previous report[18], optogenetic activation of MCH axons induced excitatory postsynaptic currents (oEPSCs) mediated by glutamate release in dLS neurons (Fig. 1f). These glutamate-mediated fast synaptic transmission consistently showed fast depression during trains of stimuli (≥ 5 Hz) (Fig. 1f,g), suggesting that glutamatergic synaptic vesicles in the MCH nerve terminal have high release probability or with a limited number of vesicles in the readily releasable pool.

The dLS is largely composed of GABAergic projection neurons, which also form an extensive yet confined recurrent axonal plexus within the dLS region, an anatomical substrate for local collateral inhibition and feed-forward inhibition (FFI)[33]. Indeed, the MCH neuron-derived oEPSCs were often followed by secondary inhibitory postsynaptic currents (oFFI-IPSCs) with a delay of a few milliseconds (Extended Data Fig. 1a,b). Therefore, during short-term stimulation (10 s; 10 or 20 Hz), the overall acute impact of MCH nerve terminal activation on dLS neuronal firing varied, depending on the net gain of excitation (i.e., oEPSCs) and inhibition (i.e., oFFI-IPSCs) (Extended Data Fig. 1c–f). There were no residual effects after the light was turned off (Extended Data Fig. 1e,f), thus ruling out any significant slow-acting peptidergic effects.

To induce MCH release and examine slow-acting peptidergic function, we used longer optogenetic stimulations compared to those required for the release of small-molecule transmitters (glutamate or GABA)[34]. We first examined changes in spontaneous action potential firing (sAP) activity of dLS neurons after prolonged optogenetic stimulation of MCH neuronal fibers in the dLS. During 80 s of 10- or 20-Hz stimulation, glutamate release was likely minimal due to fast depression (Fig. 1f,g). Among the dLS neurons with sAP (28 out of 82 neurons recorded, 2.36 ± 0.33 Hz), we observed strong suppression of sAP that was delayed by several minutes after light-train stimulations (Fig. 1h–k, Extended Data Fig. 1g,h). This suppressive effect is likely mediated by MCH signaling, as it was significantly blunted by Tc-MCH7c, a specific MCH receptor 1 (MCHR1) antagonist[35] (Fig. 1j–l). MCHR1 (the only identified functional MCH receptor expressed in the rodent brain[36]) is a G-protein coupled receptor that binds to Gαq/i3 to induce intracellular Ca^{2+} concentration increase[37]. Moreover, exogenous application of MCH mimicked the effects of optogenetic activation of MCH fibers in dLS neurons (Fig. 1j&m). These data suggest that MCH release in the dLS causes a late but prolonged suppressive effect on dLS-LHA neuronal firing and excitability.

To understand how MCH may suppress dLS neuronal firing and excitability (Fig. 1), we considered several possibilities: (1) MCH directly dampens dLS neuron excitability; (2) MCH suppresses afferent excitatory synaptic strength in the dLS, and/or (3), MCH enhances afferent inhibitory synaptic strength in dLS neurons.

MCH facilitates excitatory synaptic inputs in dLS

Despite the heavy innervation of MCH neuronal fibers (Fig. 1d), dLS neurons rarely express MCH receptors in mice[38–40]. To verify this, we performed RNAscope *in situ* hybridization using probes against MCHR1 and found few mRNAs of MCHR1 in dLS region (Fig. 2a, Extended Data Fig. 2a). Thus, direct, postsynaptic suppression of neuronal excitability by MCH via MCHR1 in dLS neurons is unlikely.

We next investigated whether MCH signaling suppresses excitatory synaptic transmission in the dLS, thus reducing the excitability of dLS neurons (Fig. 1). Both spontaneous and field electrode stimulation-evoked excitatory postsynaptic currents (sEPSCs and eEPSCs), isolated pharmacologically by application of picrotoxin (PTX), were examined in dLS-to-LHA neurons before and after optogenetic activation of MCH neuronal fibers expressing ChR2. Prolonged trains of light stimulation enhanced both sEPSCs and eEPSCs in the dLS (Fig. 2b,c, Extended Data Fig. 2b). This augmentation is likely the result of an MCH-induced increase in presynaptic glutamate release probability. Several lines of evidence support this conclusion: (1) the frequency of sEPSCs was increased (Extended Data Fig. 2b); (2) the amplitudes of both AMPA receptor (AMPAR)- and NMDAR-eEPSCs were augmented, with no change in the AMPAR-eEPSC/NMDAR-eEPSC ratio (Fig. 2b,c); and (3) there was a decrease in the paired-pulse ratio (PPR) of eEPSCs (Fig. 2d,e). The impact of optogenetic activation of MCH neuronal fibers on EPSCs in the dLS was fully abolished when MCHR1 was blocked with either TC-MCH7c[35] or SNAP94847 ref[41] (Extended Data Fig. 2c–e). Moreover, exogenous application of MCH (or its analog [Ala17]-MCH) also consistently enhanced sEPSCs in dLS neurons projecting to LHA (Extended Data Fig. 3a–c). Thus, it is likely that endogenous MCH release is induced by optogenetic stimulation, and that MCH activates presynaptic MCHR1 to enhance glutamate release in the dLS. These effects were not observed in the eYFP-expressing control (Extended Data Fig. 3d–f), thus ruling out non-specific effects of light stimulation that others have shown can alter neuronal activities[42].

To validate that endogenously released MCH is responsible for enhancing EPSCs in dLS neurons, we suppressed MCH in the hypothalamus by viral-mediated expression of short hairpin RNA targeting Pro-MCH (shRNA-Pmch). The knockdown efficiency was confirmed by MCH antibody staining after unilateral injection of shRNA-Pmch-GFP (shRNA-scramble and non-injected contralateral side used as controls; Fig. 2f, Extended Data Fig. 3g–i). To show function loss from MCH knockdown, optogenetic activation of MCH neurons with decreased (or control) MCH levels was achieved by injecting a mixture (3:1 ratio) of shRNA-Pmch (or shRNA-scrambles) and Cre-dependent AAV-C1V1-mCherry into the lateral hypothalamus of MCH-Cre mice. Expression of shRNA-Pmch-GFP reduced MCH staining compared to GFP negative MCH neurons (mCherry+) (Fig. 2g). Overall quantification demonstrated that MCH neurons infected by C1V1 (mCherry+) have

significantly decreased MCH levels in animals co-injected with shRNA-Pmch compared to shRNA-scramble (Extended Data Fig. 3j). In shRNA-Pmch group, optogenetic stimulation of MCH neuronal fibers expressing C1V1 did not lead to increased excitatory synaptic transmission or reduced PPR, whereas both effects were preserved in shRNA-scramble injected animals (Fig. 2h–k, Extended Data Fig. 3k,l).

One major excitatory input to the dLS is from dHP CA3 pyramidal neurons[25, 26], which express high levels of MCHR1 mRNA (Fig. 3a, Extended Data Fig. 4a–c). Thus, MCH could modulate CA3-to-dLS projections. Indeed, when ChR2-eYFP was expressed in CA3 pyramidal neurons, exogenous MCH doubled the optogenetically evoked HP-to-dLS excitatory synaptic strength in dLS neurons projecting to the LHA (Fig. 3b–e, Extended Data Fig. 4d,e), which was accompanied by a decrease in PPRs (Extended Data Fig. 4f). To directly address whether endogenous MCH has a similar effect, we took advantage of dual-color optogenetics. In MCH-Cre animals, we simultaneously infected MCH neurons with Cre-dependent AAV-C1V1-mCherry, in addition to AAV-CamkII-ChR2-eYFP injection in the CA3 (Fig. 3f, Extended Data Fig. 4g,h). Both eYFP-positive terminals (originating from the HP) and mCherry-positive fibers (from MCH neurons in the LHA) were observed close to the Alexa633-filled dendritic arborizations of dLS neurons recorded (Fig. 3g). Similar to what we observed after exogenous application of MCH (Fig. 3d,e), the amplitude of HP-to-dLS oEPSCs evoked by 470 nm light nearly doubled after optogenetic activation of the MCH fibers (590 nm light; 2 min at 20 Hz) (Fig. 3h,i). And, once again, the PPR of HP-to-dLS oEPSCs significantly decreased (Fig. 3j,k), suggesting presynaptic regulation is involved, likely via activation of MCHR1 expressed in CA3 axonal terminals in the dLS (Fig. 3a). The augmentation of the HP-to-dLS oEPSCs after light activation of MCH fibers was eliminated when MCH1R was blocked (with TC-MCH7c[35] or SNAP94847 ref[41]) (Extended Data Fig. 4i,j). These data strongly suggest that endogenously released MCH strengthens HP-to-dLS excitatory synaptic inputs.

Collectively, these data indicate that both exogenously applied and endogenously released MCH enhances excitatory synaptic inputs in dLS neurons, likely via a presynaptic mechanism. However, these results did not support our initial hypothesis that MCH suppresses sAPs in the dLS by suppressing excitatory synaptic strength (Fig. 1h–m).

MCH regulates inhibitory synaptic transmission in the dLS

Because the balance of excitatory-inhibitory (E/I) synaptic transmission likely accounts for the final outcome of neuronal excitability and signal integration, we explored whether MCH signaling increases the strengths of the inhibitory synaptic inputs in the dLS. Inhibitory postsynaptic currents (IPSCs) were pharmacologically isolated with CNQX and D-APV, which block excitatory synaptic transmission mediated by AMPAR and NMDAR, respectively. Under these conditions, both the frequency of spontaneous IPSCs (sIPSCs) and the amplitude of field electrode-evoked IPSCs (eIPSCs) drastically increased after prolonged optogenetic activation of MCH fibers in the dLS (Fig. 4a–d, Extended Data Fig. 5a), accompanied by a decrease in the PPR (Fig. 4c,d). These effects were fully abolished by MCHR1 blockers (Fig. 4c,d, Extended Data Fig. 5b,c), and mimicked by applying exogenous MCH (Extended Data Fig. 5d,e). Because dLS neurons rarely express MCHR1

(Fig. 2a, Extended Data Fig. 2a), these results suggest that MCH likely enhances long-range inhibitory projections from outside brain regions to inhibit the excitability of dLS neurons (Fig. 1h–m).

If MCH truly suppresses dLS neuronal excitability, local collateral synaptic strength should weaken as a result. To test this prediction, we expressed ChR2 sparsely in the dLS and recorded light-evoked intra-dLS IPSCs (oIPSCs) in neighboring non-infected dLS neurons (Extended Data Fig. 5f). Indeed, we found that the intra-dLS oIPSCs were suppressed following MCH application (Extended Data Fig. 5g,h). We next examined HP-to-dLS FFI (Fig. 4e). AAV-ChR2-eYFP was injected into the HP, and di-synaptic inhibitory response was induced by optogenetic activation of dHP-to-dLS excitatory projections (Fig. 3a). The polysynaptic nature of optogenetic-induced FFI (oFFI) was confirmed by applying CNQX, which blocks the HP-to-dLS excitatory inputs; FFI was abolished (Fig. 4f). In the presence of MCH, even though ChR2-evoked HP-to-dLS oEPSCs were enhanced (Fig. 3d,e), HP-to-dLS oFFI was found reduced (Fig. 4g,h). These data confirm that MCH suppresses dLS neuronal excitability overall, including the capacity to generate FFI.

We next investigated whether the increase in GABA tone induced by MCH signaling in the dLS is sufficient to suppress sAP firing (Fig. 1). In the presence of the $GABA_AR$ blocker picrotoxin, the suppressing effect of MCH was not fully eliminated; however, the addition of $GABA_BR$ blocker CGP55845 completely abolished the impact of MCH (Fig. 4i,j). This result suggests that a postsynaptic $GABA_BR$-mediated conductance in the dLS is key to MCH-induced inhibition. In support of this interpretation, high $GABA_BR$ expression has been identified in rodent dLS via *in situ* hybridization[43]. Moreover, $GABA_BR$-mediated conductance was isolated and directly recorded as a component of intra-dLS collateral synaptic transmission (Fig. 4k, Extended Data Fig. 5i), and of oFFI driven by HP dCA3 inputs (Fig. 4l). The kinetics of the $GABA_BR$ conductance (time-to-peak of 207.8 ± 5.9 ms) suggests the opening of GIRK potassium channels (Fig. 4k,l). In the presence of $GABA_B$ receptor blocker CGP55845, MCH failed to reduce HP-dLS oFFI, though it continuously strengthened excitatory input from the HP (Fig. 4m,n). These data indicate that $GABA_BR$-mediated inhibition during MCH modulation has a crucial role in regulating the firing of the dLS neurons.

Together these results support our hypothesis that MCH enhances inhibitory synaptic strength in dLS neurons, which is sufficient to cause a prolonged suppression of neuronal excitability and firing in the dLS.

MCH enables high-frequency neuronal spiking in the dLS

Information flow in the brain depends on neuronal spiking-activity propagation between neurons among specialized brain regions. This process is mediated by fast synaptic transmission and modulated by slower neuromodulation. Therefore, after dissecting the interactions between slow-acting MCH and fast synaptic actions mediated by glutamate and GABA, we next sought to address the overall impact of these synaptic regulatory effects on information flow at the circuit level. The dHP is well known for its role in spatial mapping[44], and uses firing rate as one of its information-coding mechanisms[45]. Most HP pyramidal cells fire at < 2 Hz while at rest, but increase their firing rate up to 50 Hz

(average 9~12 Hz) when animals are in their place fields[46–48]. Moreover, the place-mapping mechanisms of dHP are likely shared by the dLS[27, 47, 49]. Therefore, we investigated how varying the frequency of HP inputs might affect dLS neuronal spiking activity and its downstream output. We specifically examined APs evoked by light-induced dHP CA3 inputs (oAP) (Extended Data Fig. 6). During 5-s light stimulation (1 Hz), AP generation was time-locked to optogenetic stimulation of dHP CA3 inputs, with a relatively high fidelity (78.5 ± 5.13%; n=38) (Extended Data Fig. 6a–c). Spontaneous spiking activity in dLS neurons induced variability (noise) in the stimulus-locked spiking (Extended Data Fig. 6d). As the stimulation frequency increased to 5, 10, and 20 Hz, oAP production was strongly limited: during 5-Hz stimulation (25 light pulses in 5 s), approximately 13 time-locked spikes were generated in dLS neurons, which corresponds to a near 50% input-output efficiency for the HP-dLS circuit. This fell to 45% at 10 Hz and 20% at 20 Hz (Extended Data Fig. 6a–c). To identify the modulatory role of MCH while minimizing possible biases introduced by viral expression levels and/or intrinsic ChR2 failure, we reduced the laser power used to induce hippocampal oEPSCs (0.7 mW, 0.3 ms pulse width). dLS cells that had 100% spike throughput efficiency following 1-Hz stimulation were selected for further pharmacological perturbation of MCH signaling (Extended Data Fig. 7). As predicted, exogenous MCH significantly elevated the success rate of stimulus-locked spike production to over 95% at 10 Hz and 80% at 20 Hz (Fig. 5a,b). These results suggest that in the absence of MCH signaling in the dLS, spike generation in response to HP inputs is limited by shunting inhibition, especially resulted from the slow kinetic-$GABA_B$R-mediated oFFI (Extended Data Fig. 5i). Conversely, we hypothesize that when MCH is present, spike throughput increases in a frequency-dependent manner as a result of dampened $GABA_B$R-mediated FFI (Extended Data Fig. 7a,b). Indeed, blocking $GABA_B$R mimicked the effect of MCH to some extent, and also occluded the effect of MCH (Fig. 5a,b).

Together, our data strongly suggest that the dLS computes and controls information flow from hippocampal region CA3 to downstream targets, including LHA. In particular, $GABA_B$R-mediated hyperpolarization works as a biological *"*low-pass filter" to limit the transmission of higher frequency-encoded information. Through fine synaptic regulation, MCH signaling removes this filter, thus enabling information flow encoded by increased spiking rate as well as an enhanced coupling in spike timing between the HP and the dLS (Fig. 5c).

MCH in the dLS enhances HP-dependent spatial memory

Increases in spike rate and coupled of spike timing in the HP-dLS circuit are essential for spatial coding and for transforming the HP-dependent cognitive map into behavioral action[27]. As our data indicate a role for MCH in these physiological modulations, we investigated the extent to which MCH signaling controls behaviors dependent on the hippocampo-septal circuit[50].

First, in order to examine the behavioral effects mediated by MCH signaling in the dLS, we administered MCH agonist, antagonist, or vehicle into the dLS region via bilateral cannula[29] (Extended Data Fig. 8 a). Using the Morris water maze (MWM) test, we found that during memory retrieval the MCH agonist group showed increased accuracy in locating the target

area relative to the control group, whereas that of the antagonist group was marginally impaired (Fig. 6a–d). The MCH agonist group animals entered the hidden platform zone significantly more times than control animals (Fig. 6c). Animals in the MCH agonist group also spent nearly twice as long as the control group animals within the platform zone, whereas MCH antagonist group animals spent less time than controls (Fig. 6d). In contrast, these manipulations had no significant impact on distance traveled or swimming speed (Fig. 6e,f). To further examine whether pharmacological perturbations of MCH signaling in the dLS affects motor learning and skills, we conducted RotaRod tests and open-field tests. The RotaRod data suggest MCH signaling in the dLS does not affect motor learning (Extended Data Fig.8 b–e), and the travel distances and velocity were unchanged by MCH in open-field tests (Extended Data Fig. 8f–j). Moreover, in the open-field tests, the time animals spent in the center zone of the open field did not significantly change, suggesting that MCH in the dLS does not cause additional stress in mice (Extended Data Fig. 8h). The MCHR agonist group spent a significantly longer time near visually patterned walls3than control and antagonist groups. This result suggests that MCH signaling in the hippocampo-septal circuit may involve awareness and attention to environmental cues (Extended Data Fig.8 k), which is in line with the known function of MCH in controlling arousal and attention[15]. We next assayed the effect of perturbed MCH signaling on social interaction and nesting behavior, both known to be under hippocampal control[51, 52]. As the HP circuit plays an essential role in social aggression[51], we investigated whether MCH signaling in the dLS affects social interaction in mice. We found that elevated MCH signaling in the dLS mildly decreased sociability without displays of apparent aggression (Extended Data Fig. 8l–n). Because nesting and shredding behaviors are reported to be attenuated in animals with hippocampal lesions[52], we tested whether dLS MCH signaling, which modulates dHP outputs, may affect such behavior. We found that blocking MCH signaling in the dLS, impairs nesting behavior (Extended Data Fig. 8o,p), suggesting that MCH signaling may also modulate the hippocampal-dependent nesting behaviors[52].

Finally, to complement these pharmacological manipulations, we recapitulated the effect of MCH signaling on behaviors by manipulating dLS-projecting MCH neuronal activity via chemogentics (Fig. 6g–l). Cre-dependent retro-AAVs carrying Designer Receptors Exclusively Activated by Designer Drugs (DREADD) constructs, both the excitatory hM3Dq and the inhibitory hM4Di[53], were injected bilaterally into the dLS of MCH-Cre mice. Six weeks after injections, animals were tested in the MWM. Clozapine N-oxide (CNO) (1 μM) was given once to each animal by intraperitoneal injection 40 minutes prior to the training session. Consistent with the pharmacological manipulation results (Fig. 6a–f), chemogenetic activation of dLS-projecting MCH neurons enhanced the animals' ability to locate the hidden platform area, while inhibition led to impairment (Fig. 6h–j). Neither activation (hM3Dq) nor inhibition (hM4Di) of dLS MCH neurons affected their motor activity (Fig.6 k,l). Interpretation of this finding is not straightforward because chemogenetic manipulation may trigger the release of other neuroactive substances in addition to MCH, some of which may contribute to behavioral expression. However, both chemogenetic and pharmacological manipulation of MCH signaling in the dLS had similar effects on HP-dependent spatial memory (Fig. 6), supporting our conclusion that MCH signaling in the dLS enhances hippocampal-dependent spatial navigation.

Discussion

In this study, we dissected the complex synaptic- and circuit-regulatory mechanisms of neuropeptide MCH signaling in the dHP CA3-dLS neural pathway (Extended Data Fig. 9). We showed that MCH, whether exogenously applied or endogenously released, increased both excitatory (including CA3 inputs) and inhibitory synaptic strength in the dLS via presynaptic regulation of release probability. We also found that the $GABA_BR$-mediated slow inhibition has a profound impact on dLS neuronal excitability, and that intra-dLS collateral inhibition-mediated FFI limits dLS neuronal firing frequency evoked by HP excitatory synaptic inputs. MCH fine-tunes these processes to increase the dynamic range and fidelity of neuronal firing in the dLS, reflecting signal inputs from the dHP that facilitate spatial learning and memory.

Neuropeptide-containing neurons often co-release classic fast neurotransmitters in addition to neuropeptides. MCH neurons may release glutamate[18] and GABA[8], in addition to other neuropeptides, including nesfatin[16] and CART[17]. This complex neurochemistry makes it difficult to evaluate the contribution of each element to neuronal function. MCH knockout mice are lean due to increased energy expenditure[24], and animals in which MCH neurons are ablated have a similar phenotype[12]. However, MCH neuron ablation improves glucose tolerance independent of MCH[12], which is consistent with other reports that MCH may not be involved in glucose metabolism regulation[20, 21]. A more recent study indicates that glutamate release from MCH neurons underlies their role in glucose metabolism[54]. Thus, MCH and glutamate may make distinct contributions to MCH neuronal function in the brain. Our data also suggest that MCH and glutamate have different release kinetics (Fig. 1) and distinct functional impacts on downstream neuronal firing (i.e., in the dLS) (Extended Data Fig. 1 and Fig. 1). Glutamate release probability is high, so glutamate is likely depleted quickly during longer firing at higher frequency (Fig. 1f,g). MCH release likely requires longer duration and higher frequency activations[34]. Consistent with this distinction, the effects mediated by glutamate release are short-lived, whereas MCH may have more prolonged effects (Fig. 1). The differential release kinetics of classical neurotransmitters and neuropeptides might represent a common way for peptidergic neurons to control their release contents under different patterns of neuronal activity and achieve differential impacts on neuronal signaling.

Mismatches between the distributions of neuronal projections and receptor-expressing neuron bodies are widespread in both peptidergic and nonpeptidergic systems. Indeed, in mice, MCHR1 expression is not high in the dLS[38–40] (Fig. 2a), even though this area receives dense projections from MCH neurons[5, 6, 18, 25, 26] (Fig 1). This phenomenon seems to be consistent with volume release (neuroactive substances travel diffusively across a distance from the release site) for peptidergic regulation in the brain[1]. However, our detailed synaptic physiological analysis revealed that within the dLS, MCH plays a prominent role in regulating the synaptic strengths of both excitatory and inhibitory afferents. Specifically, applying MCH analogs increased the frequencies, but not the amplitudes, of spontaneous EPSCs and IPSCs; augmented the sizes of evoked IPSCs and EPSCs, accompanied by reductions in PPRs; and enhanced both AMPAR- and NMDAR- mediated EPSCs to a similar extent (Figs. 2 and 4). These synaptic modulatory effects can be mimicked with

optogenetic activation of MCH neuronal fibers and abolished by MCHR1 blockers (Fig. 4d, Extended Data Figs 2, 4 and 5), suggesting that endogenously released MCH mediates the effects on synaptic strength. Specifically, we find that MCH modulates both excitatory and inhibitory transmission in the dLS via presynaptic mechanisms. Moreover, although we found little expression of MCHR1 in the dLS (Fig. 2a), there was abundant expression of MCHR1 in the dHP CA3 (Fig. 3a), a brain region that projects strongly to the dLS. MCHR1 is likely also highly expressed in the axonal terminals of these dHP-to-dLS projecting neurons in the dLS, but *in situ* hybridization of RNA transcripts may not reveal localization at this level (Fig. 2a). Consistent with this notion, we found both exogenously applied and endogenously released MCH augmented the CA3-to-dLS excitatory synaptic inputs via a presynaptic mechanism (Fig. 3). These data clarify the conundrum of the mismatch between the distributions of MCH nerve terminal projections and apparent low MCHR1 in postsynaptic dLS neurons: MCH regulates downstream neuronal function by working on MCHR1 expressed in the CA3 nerve terminals in the dLS.

Neuronal excitability is determined by intrinsic membrane properties as well as the balance of long-range and local excitatory and inhibitory networks[3]. Both exogenously applied and endogenously released MCH augment long-range excitatory and inhibitory synaptic strengths in the dLS (Figs. 2–4). Our data also reveal that FFI, mediated by local collateral inhibition among dLS neurons, is a crucial motif used by this network for neuronal computation and information processing[55]. In HP-to-dLS transmission, the high-frequency firing of presynaptic dHP CA3 neurons does not excite postsynaptic dLS neurons to fire APs, but triggers a shutdown of postsynaptic neuronal firing. This effect is clearly dependent on the slower time course of $GABA_BR$-mediated FFI (Fig. 4; Extended Data Figs.5i and 6). Hypothalamus-originating MCH in the dLS decreases the excitability of dLS neurons and thus dampens the FFI induced by dHP excitatory inputs, thereby raising the ceiling of the dLS firing rate. This in turn increases the dynamic firing range and fidelity of dLS activity triggered by HP synaptic inputs (Fig. 5). As expected, blocking $GABA_BR$ by CGP55845 mimics the effect of MCH and also occludes further MCH effects (Fig. 5a,b). However, there are important differences (Extended Data Fig. 7). First, MCH affects both $GABA_AR$- and $GABA_BR$-mediated FFI-IPSPs, whereas CGP55845 only affects the latter. Second, MCH increases the signal-to-noise (*S*/*N*) ratio (i.e., excitatory inputs/spontaneous firings), whereas blocking $GABA_BR$ signaling increases the overall baseline activity and excitability of dLS neurons (both signal and noise). Third, to our knowledge, there is no known endogenous $GABA_BR$ antagonist in the brain. Therefore, neuropeptides such as MCH are likely to wield significant control over information processing in the hippocampo-septal circuit (Extended Data Fig. 9c). We argue that detailed synaptic mechanisms, including excitatory versus inhibitory synaptic inputs; fast versus slow synaptic transmission (e.g., $GABA_AR$ vs. $GABA_BR$ IPSCs), and neuromodulation (e.g., MCH signaling) need to be considered for their role in circuit manipulation and the control of behaviors. Understanding the nuances of synaptic signaling within a given neuronal circuit is especially important to inform experiments relying on opto- or chemogenetic manipulation to establish the neural basis of behavior. For example, in the case of dHP to dLS inputs, simply activating dHP excitatory inputs may actually dampen dLS output due to strong FFI (Extended Data Fig 6a–c). Because the MCH neurons in the hypothalamus also release glutamate in the dLS,

triggering excitation and inducing FFI (Extended Data Fig. 1), the effects of chemogenetic manipulations on behavior need to be interpreted cautiously (Fig. 6).

MCH functions in the brain likely have subgroup-, pathway-, cell type-, and species-specific functions. For example, mouse hypothalamic MCH neurons are segregated into wake-active and REM-active groups. The REM-active group projects to the HP to mediate memory erasure, whereas the wake-active group of MCH neurons likely are associated with exploration and foraging and project to other downstream regions[19]. Our data suggest that MCH neurons projecting to dLS may release MCH to regulate HP-dependent spatial memory (Fig. 6), consistent with literature suggesting MCH promotes spatial learning and memory, at least during memory acquisition and early retention[14, 15, 19, 22, 23, 29, 31]. Additionally, depending on varied downstream cell types, MCH may activate different signaling pathways because MCHR1 may couple to $G\alpha_q$ or GαI, causing either an increase in intracellular calcium or inhibition of cAMP production[37]. Our data show that MCH augments both excitatory and inhibitory afferent synaptic transmission in the dLS neurons. However, it has also been reported to suppress presynaptic release in the LHA[56]. Moreover, MCHR1 expression pattern may vary between species, as abundant MCHR1 mRNA is observed in the LS of rats[57] but not mice[39] (Fig. 2a).

The LS is one of the major downstream projection targets of the hippocampus. LS neurons in turn project to the hypothalamus and brainstem structures[26, 27, 51]. Thus, LS is an important hub for routing information from the hippocampus to other subcortical structures[27, 58]. As evidence of this, lesions within the septum impair spatial learning and memory[59]. Moreover, simultaneous *in vivo* recordings of both hippocampal and LS circuits reveal that LS neurons play crucial roles in conveying information coded by hippocampal sharp-wave ripples, which are related to memory consolidation[58] and transform the hippocampal spatial “cognitive map” for environmental cues[27]. The spatial coding information transmitted from the hippocampus to the LS is modulated by and interacts with signals related to reward in the LS[49]. Thus, elevating the dynamic range of spiking activity permits spike rate-coupling[60] and phase-coupling[46] in the hippocampo-septal circuit, both of which are essential for spatial memory[27, 44, 46, 47, 49, 60]. Our study reveals that concurrent hypothalamic-origin MCH release in the dLS modulates synaptic transmissions to increase the dynamic range of dLS neurons in response to hippocampal inputs, thus strengthening rates- and phase-relations between the HP and the dLS. In this way, MCH signaling the dLS may facilitate working memory associated with enhanced spatial accuracy guided by environmental cues[48, 49]. How MCH affects LS high-frequency oscillations and regulates hippocampal ripples at the systems level using *in vivo* recordings or imaging techniques remains to be explored.

Our data reveal important insights into the neuronal basis of MCH function in the HP-dLS neurocircuit. Specifically, we show that MCH released in the dLS contributes to facilitating spatial memory formation via impacts on synaptic transmission modulated by HP output. Thus, we posit a mechanism linking hypothalamic activity and HP outcome. Specifically, through MCH neurotransmission, HP output can influence behavior in a state-dependent manner, facilitating behavioral adjustments in response to energy or hormonal status, environmental factors, or social threats—all of which involve hypothalamic signaling.

Methods

Animals

All procedures involving mice were approved by the Rutgers Robert Wood Johnson Medical School Institutional Animal Care and Use Committee (IACUC). All the animals used in this study were 5–16 week-old males unless otherwise stated. The animals are bred in the facility, which is maintained at ~22°C and 35%–55% humidity. The MCH-Cre transgenic mice and wild-type mice (C57BL/6) were initially purchased from Jackson Laboratory. Mice were group housed except when otherwise stated and maintained on a 12-hour light/dark cycle (lights on at 6:00 A.M.) with food and water available *ad libitum*.

Retrograde Labeling

Mice (8 weeks old) were anesthetized using isoflurane and placed in a stereotactic frame (KOPF M1900). Standard serological and injection procedures were followed as described previously[61]. Red or green RetroBeads (100 nl, LumaFluor) were injected unilaterally into the dLS. Coordinates: Anteroposterior (AP): +0.5 mm, mediolateral (ML): ±0.45 mm, and dorsoventral (DV): −2.7 mm) or LHA (AP: −1.2 mm, ML: ±1.0 mm, and DV: −5.1 mm). Animals were allowed to recover in their home cages for 14 days to allow adequate retrograde transportation of the beads to the soma of input neurons. Injection sites were verified in all post-mortem animals.

Virus infection

The AAV-viruses used in this study include: AAV-EF1a-DIO-ChR2-YFP, rAAV2/CamKII-ChR2(H134R)-EYFP-WPRE-PA, AVV-EF1a-DIO-C1V1(E122T/E162T)-TS-mCherry, AAVrg-hSyn-DIO-hM3D(Gq)-mCherry, AAVrg-hSyn-DIO-hM4D(Gi)-mCherry, AAVrg-sSyn-DIO-mCherry. All were purchased from the University of North Carolina Vector Core or Addgene. The ChR2-YFP encodes a membrane-bound fusion protein, allowing visualization of both the cell bodies and axons of infected neurons. Viral-mediated protein expression was allowed for a period of 6 weeks prior to experimental manipulation. Injection sites were confirmed in all post-mortem animals reported in this study. 0.6–1 μL virus was used for the injection of the Cre-dependent expression AAV virus. For the non-Cre dependent AAV virus, 0.2–0.4μL of virus was injected. The injection speed was 0.1 μL/10 min and the injection coordinates for HP were: AP: −1.6 mm from bregma; ML: ± 1.8 mm; DV: −2.2 mm; for the LHA and dLS, same as the above mentioned. Six weeks post-surgery, mice were deeply anesthetized with Euthasol, decapitated and brains were quickly removed from the skull. Coronal dLS or LHA slices (300 μm) were prepared and whole cell patch clamp recordings were performed.

The AAV/DJ-m-Pmch-shRNA-GFP and control shRNA AAV-DJ-GFP-Scramble control were generated by Vector Biolabs. The Pmch-shRNA target sequence is “ACGAGAGCGGTTTCATGAA”. Knockdown or control viruses together with AAV-C1V1-mCherry viruses (Addgene) were injected into the LHA region at 3:1 ratio. Slice physiology were conducted 5–6 weeks after injections.

RNAscope in-situ Hybridization

To detect the mRNA molecules of MCHR1 and vGAT, standard protocol suggested by the manufacturer (ACDBio) was followed. RNAscope™ Fluorescent Multiplex Reagent Kit was used. RNAscope® Probes used were: Mm-Mchr1, Mm-Slc32a1 (vGAT), Mm-Ppib (Positive control probe) and DapB (Negative control probe). Briefly, fresh frozen brain samples were obtained from wildtype animals, cut into 15 μm slices by cryostat, and mounted on slides. Slides containing dorsal hippocampus or dorsal lateral septum were fixated (15 min 4% paraformaldehyde) and dehydrated (50%, 70% and 100% ethanol, 5 min each) before proceeded immediately to the RNAscope assay. Mn-Mchr1 and Mm-slc32a1 were assigned to different fluorescent channels. Both positive and negative control probes were used to control the specificity of signals. Confocal images were taken by using Zeiss LSM700 or LSM800. RNAscope® mRNA signal quantifications were done according to the ACDBio Guideline on how to quantify RNAscope® Fluorescent Assay using ImageJ.

In vitro *Electrophysiology*

Mice were anesthetized, decapitated, and brains were removed and quickly immersed in cold (4°C) oxygenated cutting solution (containing in mM: 50 sucrose, 2.5 KCl, 0.625 $CaCl_2$, 1.2 $MgCl_2$, 1.25 NaH_2PO_4, 25 $NaHCO_3$, and 2.5 glucose, pH 7.3 with NaOH). Coronal hypothalamic or dLS slices, 300 μm in thickness, were cut using a vibratome (VT 1200S; Leica). Brain slices were collected in artificial cerebrospinal fluid (ACSF) and bubbled with 5% CO_2 and 95% O_2. The ACSF contained (in mM): 125 NaCl, 2.5 KCl, 2.5 $CaCl_2$, 1.2 $MgCl_2$, 1.25 NaH_2PO_4, 56 $NaHCO_3$, and 2.5 glucose (pH 7.3 with NaOH). After at least 1 hour of recovery, slices were transferred to a recording chamber and constantly perfused with bath solution (30°C) at a flow rate of 2 ml/min. Whole cell patch clamp recordings were performed as described elsewhere[13], using pClamp version 10.7.0.2 for data collection Briefly, patch pipettes with a resistance of 4~6 MΩ were made from borosilicate glass (World Precision Instruments) with a PC-10 Narishige puller and filled with a solution containing (in mM): 126 K-gluconate, 4 KCl, 10 HEPES, 4 Mg-ATP, 0.3 Na_2-GTP, 10 phosphocreatine, (pH to 7.2 with KOH) or 90 K-gluconate, 40 CsCl, 1.8 NaCl, 1.7 $MgCl_2$, 3.5 KCl, 0.05 EGTA, 10 HEPES, 2 Mg-ATP, 0.4 Na_2-GTP, 10 phosphocreatine, 5 mM QX314 (pH to 7.2 with CsOH). Dextran Alexa Fluor 633 was included in the intracellular recording solution for cell labeling. After whole cell patch clamp was achieved, evoked EPSCs were recorded in voltage clamp at −70 or +40 mV in the presence of PTX (50 μM) to dissect specific AMPAR and NMDAR components. IPSCs were recorded under voltage clamp at either −70 mV with CNQX (20 μM) or 0 mV, according to the pipette solution used. For all field stimulation-induced responses, the electrode was placed at least 125 μm laterally from the recorded neuron; a model 2100 Isolated Pulse Stimulator (A-M Systems) was used to generate stimulus. For the optical activation of ChR2-positive fibers, a LED light source was used to generate 470nm blue light with 1000 mA power and 1ms pulse width, except when otherwise stated. Input resistance and series resistance were monitored throughout the experiments, and recordings were rejected if series resistance increased to above 25 MΩ, which would cause voltage holding error and thus inaccurate current responses kinetics and amplitudes. Pharmacological agonists/antagonists were applied via perfusion into the bath recording solution after control recording. All data were sampled at 5 kHz and analyzed offline using ClampFit 10.2 (Molecular Devices, USA). For graphical

representation, the stimulus artifacts were removed. MCH, TC-MCH 7c, SNAP 94847, [Ala)-MCH, Cart, PTX, TTX, D-APV, and QX-314 were obtained from Tocris Inc (USA); MCH (H-070–47) antibody was obtained from Phoenix Pharmaceutical and used 1:1000 dilution.

Integrated to a section at the endIntra-dLS cannula implantation and behavior tests

Cannulation was performed as previously described. Briefly, total 30 male C57BL/6 wild-type mice at 6 weeks of age, were anesthetized and implanted with bilateral guide cannulas with dummy injectors (PlasticsOne) targeting the dLS region; coordinates: AP: +0.45 mm, ML: ±0.35 mm, and DV: −2.4 mm. Mice were group housed (cannula were protected by capping) for 5 weeks to allow recovery from the surgery, during which daily food intake and body weights were monitored. Total 5 animals were removed during recovering or testing due to loosening of implant or body weight drop. All behavioral testing was conducted blindly, between 6 AM and 12PM, arranged in order of least disruptive (absence of noxious stimulation, i.e., social interaction, open field/object recognition task, and RotaRod) to most disruptive (involving physical stimuli, i.e., MWM). Animals were handled and infused PBS bilaterally (100nl, 3 days) through an injector (with 0.2 mm extra in length) before a behavior test to allow adaptation. Posthoc verification of implantation was conducted after the completion of behavior tests. Animals were sacrificed and fixed by 4% paraformaldehyde via transcardial perfusion. 200 μm brain slices were cut using a cryostat, and tracks of cannula and injector tips were clearly viewed under a stereo microscope. Data from 2 mice with incorrect placement of the cannula were excluded from the data analysis. For chemogenetics manipulated MWM test, posthoc verification of viral expression in the LHA was performed with 100 μm brain slices. Data from 1 animal in the hM3Dq and 2 animals from hM4Di groups were removed from analysis due to weak viral expression.

Social interaction test was designed to analyze the amount of time a subject mouse spends in 1 side of a test cage (chamber 1) containing a confined familiar mouse, versus the other side (chamber 2) containing a confined stranger mouse. The animal movement trajectory was monitored and analyzed with the Afasci Smartcage® system. The dependent variable was the percentage of time the test mouse spent within a given compartment. The confining cages were made of stainless wire mesh, each fixed on the opposing walls. Five minutes were given to each experimental subject to explore and habituate to the environment with both wire cages left empty. Next, one random male mouse was introduced to the experimental subject and placed in chamber 1 for 10 min; chamber 2 was left empty. Finally, the experimental subject was tested again, this time the initial mouse was used as the “familiar” and a second, novel mouse (similar age and matching sex) was added to chamber 2.

The open field/object recognition test addresses both non-specific and stimulus-specific exploratory behavior[62]. Subjects were placed in a 56×62 cm empty open field and allowed to explore. Two sidewalls were patterned differently with stripes or dots, whereas the other two sidewalls had no pattern. Paths of locomotion and time spent in specific areas of the test field were recorded by a camera and analyzed using the Anymaze software.

RotaRod test consisted of three trials (30min intertrial interval) per day over the course of 4 days. Each trial ended when the mouse either fell off or stayed on for 300s. For the first 10 trials, the RotaRod accelerated from 4–40 revolutions/min in 300s. For the last 2 trials, the RotaRod accelerated from 4–40 revolutions/min in 150s. The time to either fall off the rod or turn one full revolution was measured.

Nesting behavior[63] was measured by giving a new 5 cm × 5 cm square of pressed cotton material in 1 cage for each animal every day after the completion of the daily RotaRod trial. The resulting nest was scored the next morning using an arbitrary 5-point scoring method.

The Morris water maze test is a standard test of spatial learning and reference memory. As described before[64], an expedited form of the test was run over two days, with the first day consisting of 7 or 12 acquisition trials, while the second day involved a probe test. The MWM pool was 110cm in diameter and filled with water kept between 21° and 23°C. During the acquisition phase, a small, round platform was hidden 1–2 cm below the surface. The water was made opaque with non-toxic colored paint (white or black) to ensure the platform was not visible. Permanent cues were located on a dark plastic curtain around the enclosed pool. The curtain served to hide the experimenter who operated the computer running the tracking software. In practice, the pool was divided into four quadrants, and each subject always started from a random quadrant that did not house the platform (always oriented to face the pool edge). Each training trial was a maximum of 60s. If the subject found the platform within 60s, it was left to sit on the platform for 10s and was then removed. If the subject did not find the platform at the end of the 60s, it was placed on the platform and allowed to sit for 20s before being removed. There was a 20-minute inter-trial interval between each of the twelve trials spent in the home cage. Twenty-four hours later, the platform was removed for the 120s probe trial. The percent time spent in the target quadrant where the platform was hidden during acquisition trials and absolute time passing through the hidden platform region were used as the dependent variables for the probe test.

Experimental design, Statistics & Reproducibility

For in vitro electrophysiological experiments, each recorded neuron came from one brain slice of one experimental animal. No repeated use of each brain slice. In each experiment, the set of data points came from three or more animals, and were pooled for analysis. These experiments were not performed blindly. For RNAscope *in-situ* Hybridization, three or more animals were used for each parameter and the data of all slices were pooled for statistical analysis. These experiments were not performed blindly. For behavioral tests, data were collected and analyzed using AnyMaze version 6 (ANY-maze, UK) and CageScore2 (Afasci, Inc, USA) Each cannulated animal received one of the treatments only; mice received chemogenetic manipulation were all injected with CNO. Behavioral experiments were performed blindly. All histological, immunohistochemical and RNAscope experiments were carried out more than three times in at least three animals to ensure the reproducibility of the experiments.

For all experiments, statistical analysis was performed using Graphpad Prism 9 and the statistical methods are stated in the figure legends. All statistical tests were two sided and adjustments were made for multiple comparisons. No statistical methods were used to

predetermine sample sizes, but our sample sizes are similar to those reported in previous publications[13, 42,51,56,61]. Data distribution was assumed to be normal but this was not formally tested. Data are presented as mean ± SEMs. Individual data points are plotted in figures. Descriptions of statistical analysis are provided in the main text and each figure legend.

Data Availability

All data are contained in the main text, extended data or supplementary information. Source data can be downloaded at https://figshare.com/s/608dcd5f1a9d5a1d60df

Code Availability

No custom code is used in this study.

Extended Data

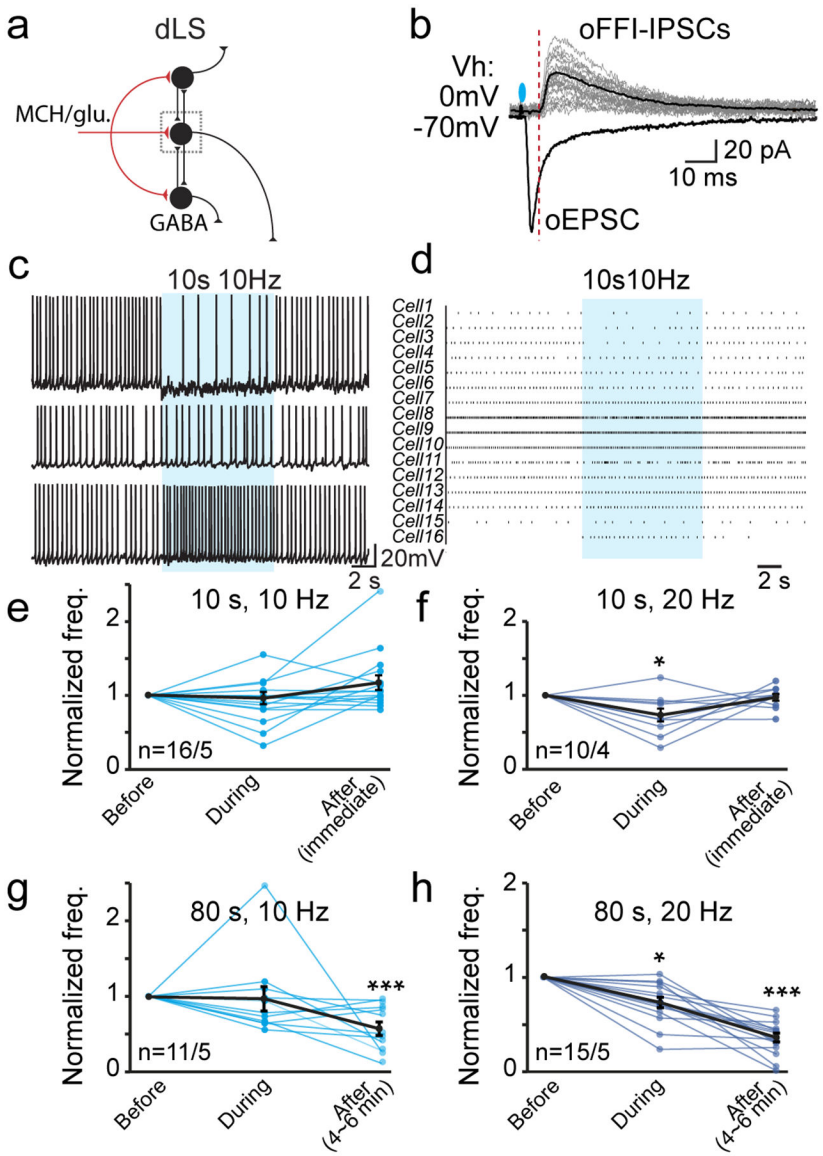

Extended Data Fig. 1. Optogenetic stimulation of LHA MCH-dLS may induce immediate impact on spontaneous dLS neuronal firing.

a, Wiring diagram of possible dLS neurocircuitry. **b**, Sample traces of optogenetically-induced oEPSCs and feed-forward-inhibitory oIPSCs. **c**, Representative traces of dLS neuronal spontaneous action potentials (sAPs) before, during, and after 10 s optogenetic stimulation of MCH fibers. **d**. Raster plot of sAPs. **e-h**, Normalized and pooled data of dLS neuronal firing under 10s or 80s, 10Hz or 20Hz stimulation. Data are mean ± SEM; numbers of neurons/animals analyzed are indicated. Paired two-tailed Student's t-tests were used, e, before vs. during p=0.622758; before vs. after p=0.109378; f, before vs. during p=0.01251; before vs. after p=0.575929; g, before vs. during p=0.0.875236; before vs. after p=0.000832; h, before vs. during p=0.000201; before vs. after $p=1.25\times10^{-9}$. * p<0.05, ** p<0.01, ***p<0.001.

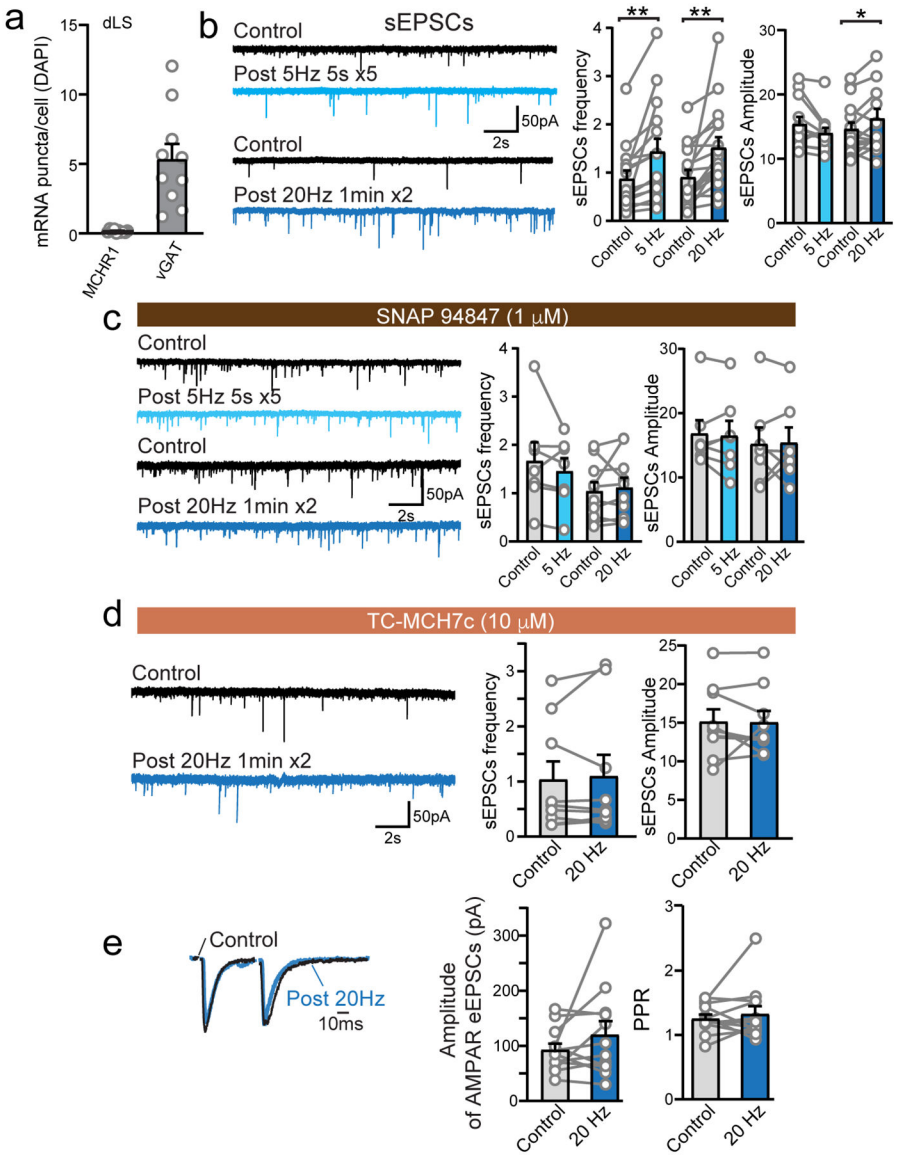

Extended Data Fig. 2. MCH enhances excitatory transmission in dLS-to-LHA projecting neurons via a presynaptic mechanism.

a, Quantification of mRNAs of MCHR1 or vGAT in the dLS.n=10**. b**, Sample traces of sEPSCs before and after trains of optogenetic activation of MCH fibers (*left panel*); *right panel*, Pooled data of the comparisons of frequencies and amplitudes of sEPSCs. n=15 cells/8 animals and 16/9 cells/animals, at 5Hz and 20Hz, respectively. Paired Student's t-tests were used: sEPSC frequency: Control vs. Post 5 Hz p=0.0053; Control vs. Post 20 Hz p=0.0051; sEPSC amplitude: Control vs. Post 5 Hz p=0.0533; Control vs. Post 20 Hz p=0.047. **c**, Sample traces of sEPSCs before and after optogenetic activation of MCH fibers in the presence of SNAP94847; *right panel*, Pooled data of the comparisons of frequencies and amplitudes of sEPSCs. n=7 cells/3 animals and 10/4, at 5Hz and 20Hz, respectively. Student's t-tests were used: sEPSC frequency: Control vs. Post 5 Hz p=0.3281; Control vs. Post 20 Hz p=0.5684; sEPSC amplitude: Control vs. Post 5 Hz p=0.6994; Control vs. Post 20 Hz p=0.8967. **d&e**, In the presence of Tc-MCH7c, no changes in spontaneous (d)

or evoked EPSCs (e) were observed post 20Hz optogenetic stimulation of MCH fibers.n=9 cells /4 animals (d), 12/4 (e). Student's t-tests were used: d, sEPSC frequency, Control vs. Post 20 Hz p=0.584; sEPSC amplitude, Control vs. Post 20 Hz p=0.9283; e, eEPSC amplitude, Control vs. Post 20 Hz p=0.2007; PPR, Control vs. Post 20 Hz p=0.4978. Data are mean ± SEM, * p<0.05, ** p<0.01, ***p<0.001.

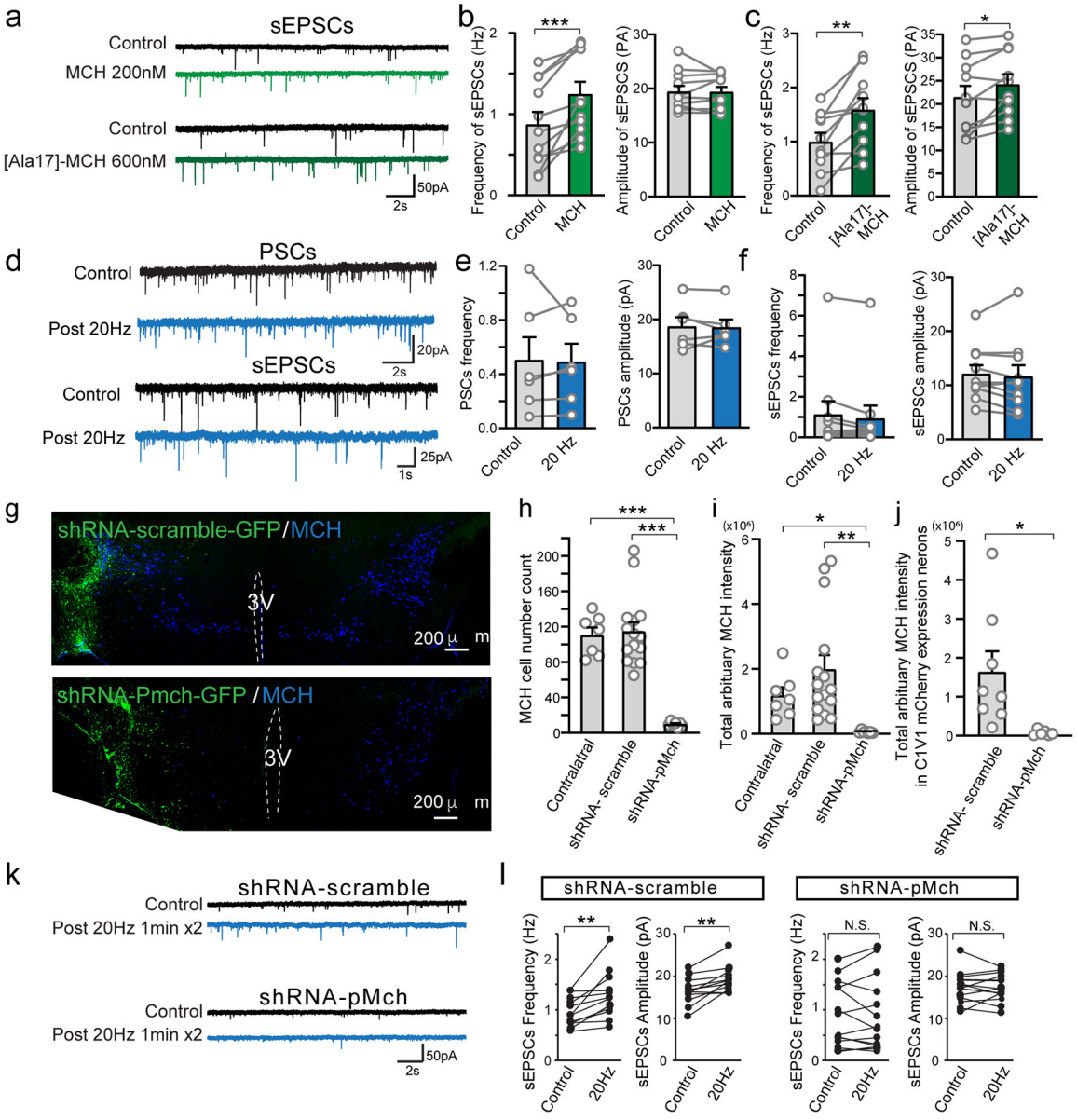

Extended Data Fig. 3. MCH regulates excitatory transmission in dLS neurons.

a-e, Impact of exogenously applied MCH and [Ala17]-MCH on sEPSCs, showing representative traces (**a**) and pooled data (**b-e)**. n=11 cells/6 animals for b&c; and 10/3 for d&e. Paired two-tailed Student's t-tests were used: b, frequency p=0.0006, amplitude p=0.936; c, frequency p=0.0025, amplitude p=0.021.**d-f**, Expression of eYFP in MCH neurons after optogenetic stimulation does not impact synaptic transmission. **d**, Sample

traces of PSCs and sEPSCs before and after trains of optogenetic stimulation (20Hz 1 min × 2) of MCH fibers expressing eYFP. **e&f**, Pooled data of the normalized frequency or amplitude of PSCs (e) and sEPSCs (f). Data are mean ± SEM; n=6 cells/3 animals for e; n=11/3 for f. Paired two-tailed Student's t-tests were used, no statistical significances were found. For PSCs, Frequency p=0.8676, Amplitude p=0.8205; for sEPSCs, Frequency p=0.0717, Amplitude p=0.4319. **g-l**, Knockdown of MCH abolish the regulatory effects after optogenetic activation of MCH neuronal fibers in the dLS. **g**, Sample images of tissue following unilateral injections of shRNA AAVs shRNA-scramble or shRNA-Pmch viruses. **h&i** Quantification of MCH neurons and MCH immunofluorescent signal in the hypothalamic area after shRNA knockdown of pMch. n=7, 15, 7, in contralateral, scrambled and shRNA-pMch groups, respectively. h, Welch's AN OVA tests were used, $F(2,11.45)=109.8$, $p<0.0001$. Contralateral vs. shRNA scramble p=0.9845, Contralateral vs. shRNA-pMch $p<0.0001$, shRNA-scramble vs. shRNA-pMch $p<0.0001$. I, Welch's ANOVA tests were used, $F(2,11.27)= 18.22$, p=0.0008, Contralateral vs. shRNA scramble p=0.3187, Contralateral vs. shRNA-pMch p=0.0133, shRNA-scramble vs. shRNA-pMch p=0.0016. **j**, Quantification of MCH immunofluorescent signal in cells with expression of C1V1-mCherry. n=8,6, in Scrambled shRNA and shRNA-pMch groups. Unpaired Student's t-test, p=0.0266 **k-l**, Impact of MCH shRNA AAV (or control scrambled shRNAs) on the modulatory effect of post-optogenetic stimulation of sEPSCs, showing representative traces (**k**) and pooled data (**l)**. n=12, 14 for l in shRNA-scramble and shRNA-pMch groups, respectively. Paired Student's t-tests were used, shRNA-Scramble: Control vs. post 20Hz, Frequency p=0.003531; Amplitude p=0.001719; shRNA-pMch; Control vs. post 20Hz, Frequency, p=0.0.998361, Amplitude, p=0.95653. Data are mean ± SEM; * $p<0.05$, ** $p<0.01$, *** $p<0.001$.

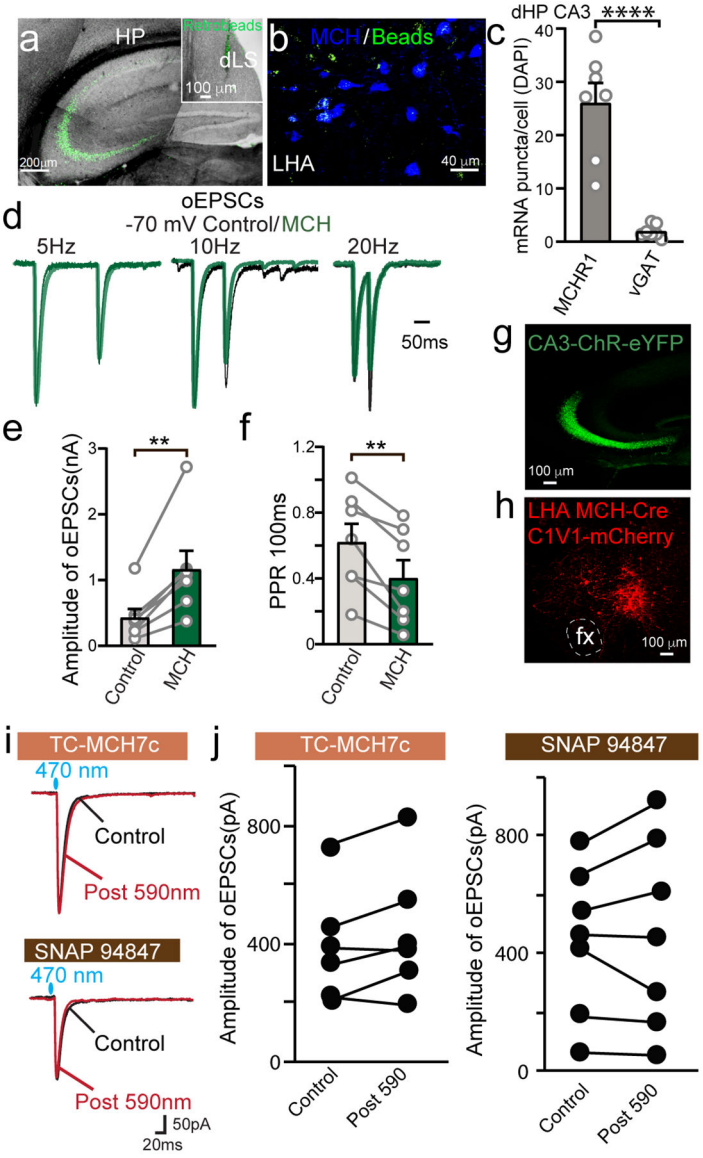

Extended Data Fig. 4. MCH facilitates hippocampal excitatory inputs to dLS neurons.

a, Sample images of retrograde labeled CA2/3 neurons after microfluorescent RetroBeads were injected into the dLS region. **b**, Retrograde labelled LHA neurons (green) with immunoreactivity for MCH (blue). **c**, Quantification of mRNA of MCHR1 and vGAT in the dorsal hippocampal CA3 region. n= 7, unpaired Student's t-test, p<0.0001. **d**, Sample oEPSCs evoked by paired-pulse protocols at different intervals before (control) and after the application of MCH. **e&f**, Quantification of oEPSCs originating from hippocampus in dLS neurons before and after the application of MCH. Data are mean ± SEM; n=7 cells/3 animals for e & f. Paired two-tailed Student's t-tests were used: e, p=0.0031; f, p=0.0033 ** p<0.01. **g&h**, Sample images of injection sites. **i&j** Endogenous MCH facilitates HP-to-dLS EPSCs via MCHR1 signaling. **i**, Representative superimposed traces of optogenetically-induced EPSCs in the dLS, in the presence of TC-MCH7c (10 μM) or SNAP94847 (20 μM), pre- (black trace) and post- (red trace) prolonged 590nm light activation on C1V1-positive

MCH axons. **j**, Pooled single oEPSC amplitude data. Paired two-tailed Student's t-tests were used but no statistical differences were found, p=0.0907 in TC-MCH7c and p=0.6607 in SNAP94847.

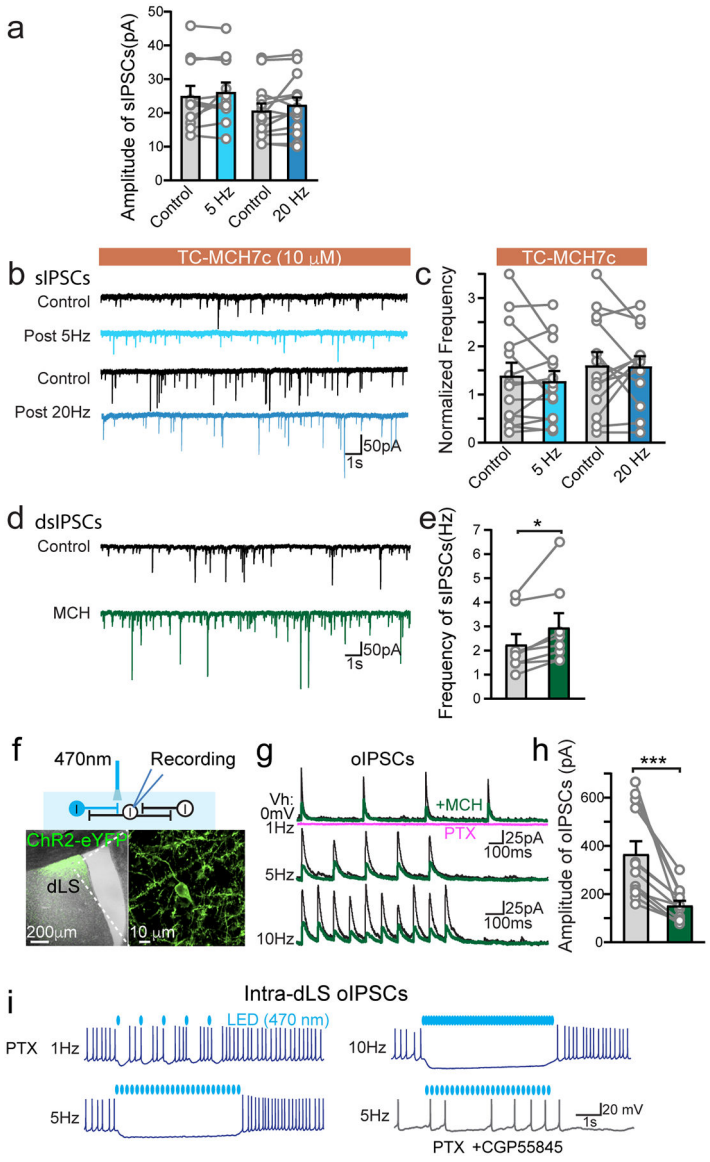

Extended Data Fig. 5. Endogenous MCH increases GABA tone in the dLS.

a, Pooled data for amplitude. n=11 cells/9 animals and 14/9 for 5 Hz and 20Hz, respectively. Paired two-tailed Student's t-tests were used: 5Hz, p=0.2905 and 20Hz, p=0.132. AAV-DIO-ChR2-eYFP was injected into the lateral hypothalamic region of MCH-Cre mice, sIPSCs (isolated pharmacologically in the presence of CNQX and APV) were recorded in dLS neurons. MCH fibers were optogenetically activated using two different paradigms (5 Hz 5 second × 5 or 20Hz 2min). sIPSCs were recorded before optogenetic stimulation (Control) and 2–3 min after optogenetic stimulation (indicated as 5Hz or 20Hz). **b**, Sample traces showing the impact of optogenetic stimulation of MCH fibers on sIPSCs in dLS neurons,

as described above, in the presence of Tc-MCH7c. **c**, Pooled data show that in the presence of TC-MCH7c, the facilitatory effects induced post-prolonged optogenetic stimulation of MCH fibers were abolished, suggesting the involvement of MCH signaling. n=14/7 and 13/7 for 5Hz and 20Hz, respectively. Paired two-tailed Student's t-tests were used: 5Hz, p=0.4489 and 20Hz, p=0.9195. **d**, Sample traces of sIPSCs in the absence (Control) or presence of MCH. **f**, Pooled data for e. n=8/4 neurons/animals. Paired two-tailed Student's t-tests were used, p=0.0198. **f-h** MCH suppresses collateral transmission in the dLS. **g**, Diagram of experimental setup and sample images showing AAV-ChR2-eYFP infection in the dLS. Whole-cell patch clamp recordings were made from cells without ChR2-eYFP infection in the dLS; fibers and neuronal cell bodies expressing ChR2 were activated by 470 nm LED light (each pulse at 1ms duration at 1, 5 and 10 Hz); collateral optogenetically-induced IPSCs were recorded. **g**, Sample traces showing the $GABA_AR$-mediated inhibitory collateral synaptic transmission before (black traces) and after (green traces) administration of exogenous MCH (600nM) through perfusion chamber. **h**, Pooled data from b. n=12 cells/5 animals. Paired two-tailed Student's t-tests were used, p=0.0006. **i**, $GABA_B$ receptor-mediated inhibition suppresses spontaneous firing of dLS neurons. Sample traces showing that $GABA_B$ receptor-mediated inhibitory synaptic transmission is sufficient to suppress dLS spontaneous action potential firing. AAV-ChR2-eYFP was injected into the dLS. Whole-cell patch clamp recordings under current clamp mode were made from cells without ChR2-eYFP infection in the dLS; fibers and neuronal cell bodies expressing ChR2 were activated by 470 nm LED light (each pulse was 1ms duration delivered at 1, 5 or 10 Hz). In the presence of $GABA_AR$ blocker PTX, optogenetic stimulation delivered at varying frequencies (1Hz, 5Hz and 10Hz) to activate dLS neurons suppressed spontaneous firing. Higher frequencies produce prolonged hyperpolarization in dLS neurons. In the presence of CGP55845, a $GABA_BR$ blocker, the suppression of firing and hyperpolarization of membrane potential were both blocked, suggesting the involvement of $GABA_B$ receptor signaling. Data are mean ± SEM * $p<0.05$, ** $p<0.01$, *** $p<0.001$.

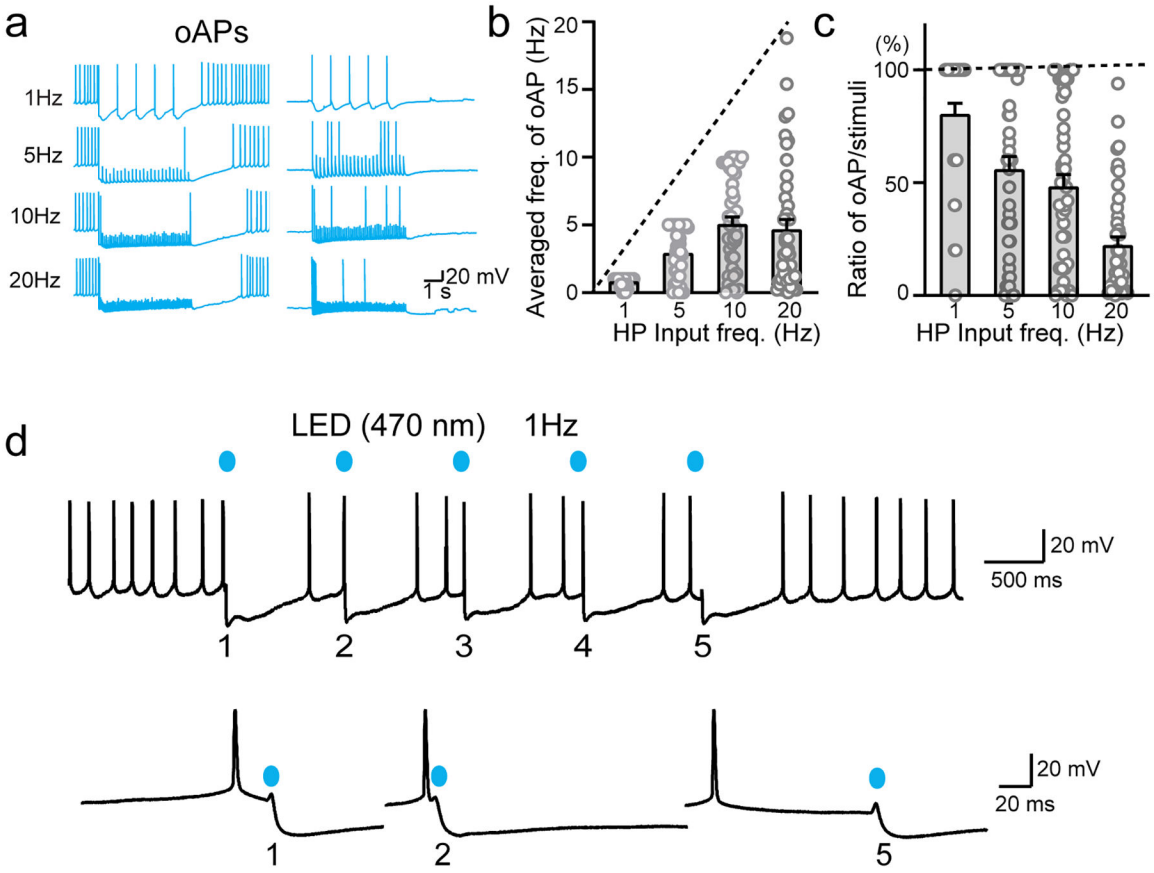

Extended Data Fig. 6. $GABA_BR$-mediated FFI functions as a low-pass filter.

The FFI acts as a gate to block high-frequency-encoded information generated in the hippocampus from passing through to downstream targets through the dLS neural network. **a**, Sample traces of dLS neuron firing in response to optogenetically-evoked oEPSCs from the dHP. **b&c**, Pooled data from **a**. **d**, Sample traces of neurons firing spontaneous APs interferes with 1Hz dHP excitatory inputs induced AP generations. n=38 cells/ 9 animals. Data are presented as mean ± SEM.

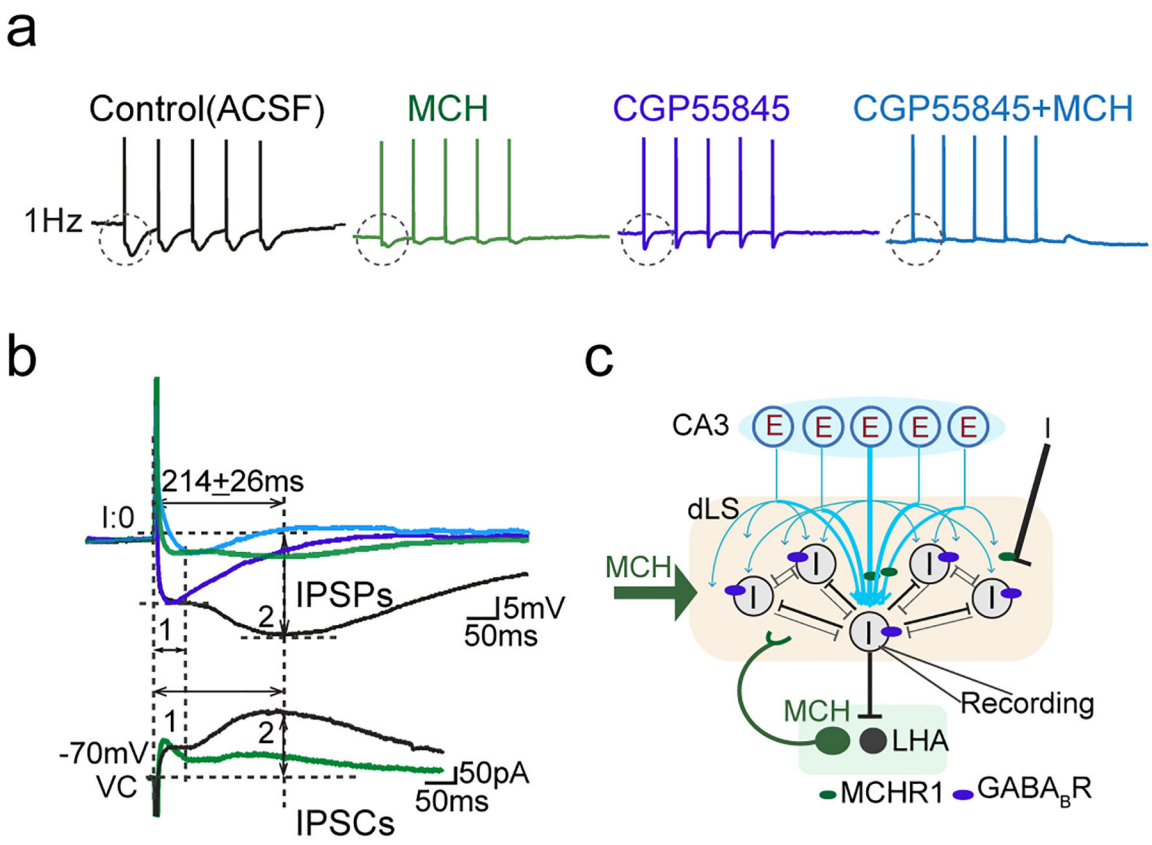

Extended Data Fig. 7. Hippocampal inputs induced postsynaptic action potentials.

a, Sample traces of neuronal oAPs induced by 1Hz dHP excitatory inputs. **b**, Superimposed postsynaptic potentials (*upper panel*) and postsynaptic currents (*lower panel*) under different conditions (indicated by different color as indicted in **a**). **c**, Diagram of possible wiring of HP-dLS-LHA neurocircuitry

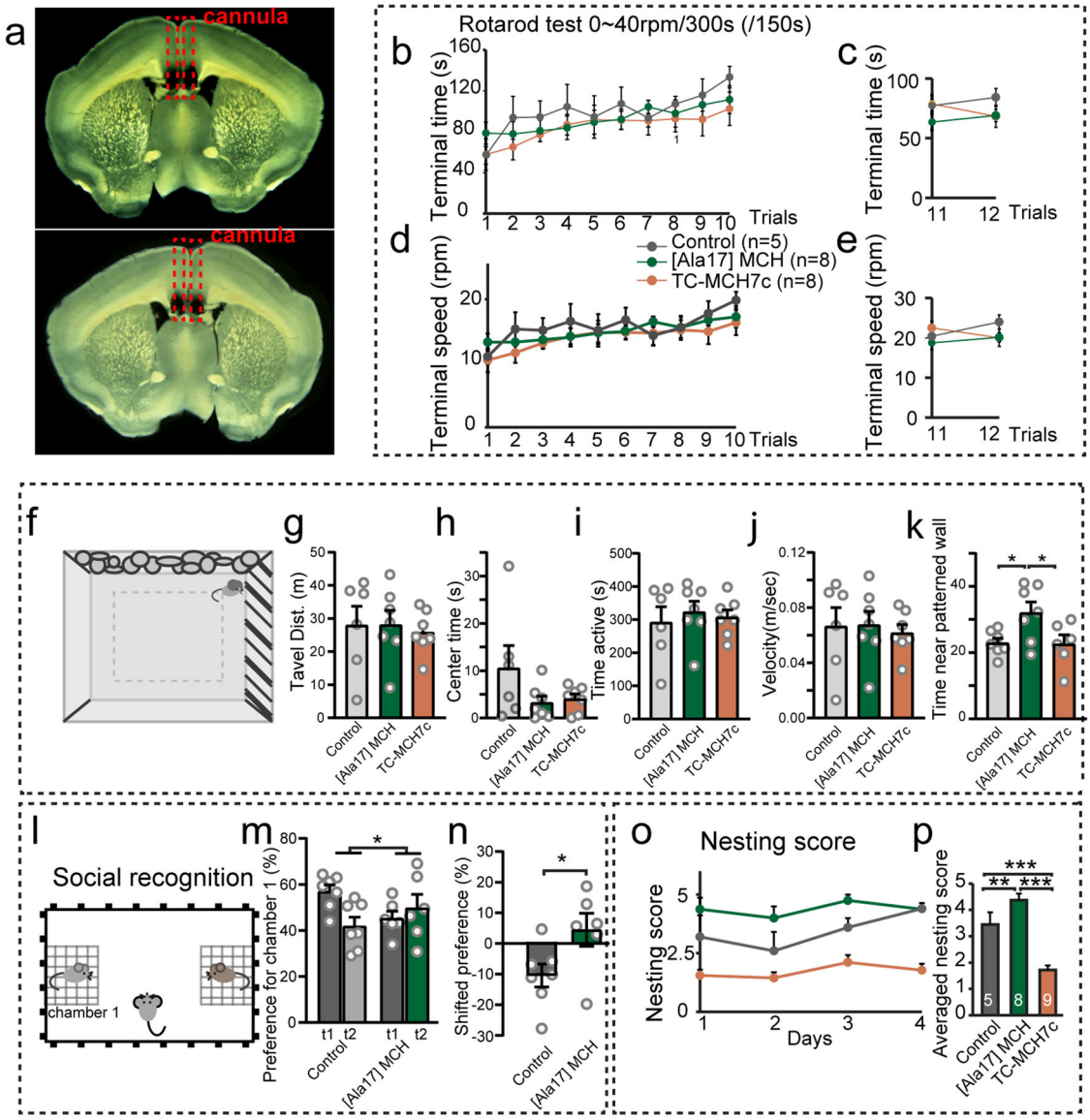

Extended Data Fig. 8. Behavioral impacts of MCH signaling in the dLS.

a, Light microscope image of sample coronal brain slices illustrating the guide and internal cannula tracks. Tracks of injector tips are labeled by stars. **b-e**, RotaRod Motor learning task data. **b&d**, pooled data for the first 10 trials, in which speed accelerated from 4–40 revolutions/min in 300s. Two-way ANOVA test was used. **b**, animals x treatment p=0.9602, treatment p=0.464. **d**, animals x treatment p=0.9509, treatment p=0.5329. **c&e**, Pooled data from the last 2 trials, in which speed accelerated from 4–40 revolutions/min in150s. Two-way ANOVA test was used. **c**, animals x treatment p=0.1222, treatment p=0.2944. **e**, animals x treatment p=0.0776, treatment p=0.4157. **f-k**, Performance on the locomotor open field test with patterned wall. n=6,7,7 in control, MCH and Tc-MCH7c groups. One-way ANOVA test with *posthoc* Tukey's multiple comparison were used for all analysis. **f**, Schematic of the testing arena. **g**, Distance traveled under each treatment condition. F(2,17)=0.1059,p=0.9001. **h**, Time spent in center time under each treatment condition.

Treatment F(2,17)=2.124, p=0.1501. **i**,Time spent active under each treatment condition. Treatment F(2,17)=0.2081, p=0.8142. **j**, Movement velocity under each treatment condition. treatment F(2,17)=0.1037, p=0.902. **k**, Time spent near patterned walls under each treatment condition. Treatment F(2,17)=4.522, *p=0.0.0266; Control vs. Ala17]MCH, p=0.0477, [Ala17]MCH vs. TC-MCH7c, p=0.0482. **l-n** Social recognition behavior with or without MCHR1 agonist. Metric=time (%) spent in the side of each chamber (Chamber 1: familiar mouse; Chamber 2: novel mouse). **m**, Preference for chamber 1: Two-way ANOVA test was used for statistics, F(1,11)=8.459, p=0.0142. **n**, Data showing a shifted preference, n=7 and 6 in control and MCH groups, respectively. Unpaired Two-tailed Student's t-test was used: p=0.04. **o&p**, Nesting behavioral analyses. Metric = arbitrary nesting scores. **o**, Two-way ANOVA test with *posthoc* Tukey's multiple comparison were used for statistics, treatment x day F(6,44)=0.7998, p=0.5754, treatment F(1.985, 43.68)=67.51, p<0.0001; Control vs. [Ala17]MCH p=0.0106, Control vs. TC-MCH7c p<0.0001, [Ala17]MCH vs. TC-MCH7c, p<0.0001. **p**, Average nesting score over 4 days. F(2,19)=30.36, p<0.0001. *Posthoc* Tukey's multiple comparison, Control vs. MCH, p=0.0096; Control vs. TC-MCH7c, p<0.0001; MCH vs. TC-MCH7c, p<0.0001. Data are presented as mean ± SEM, * p<0.05; ** p<0.01, *** p<0.001

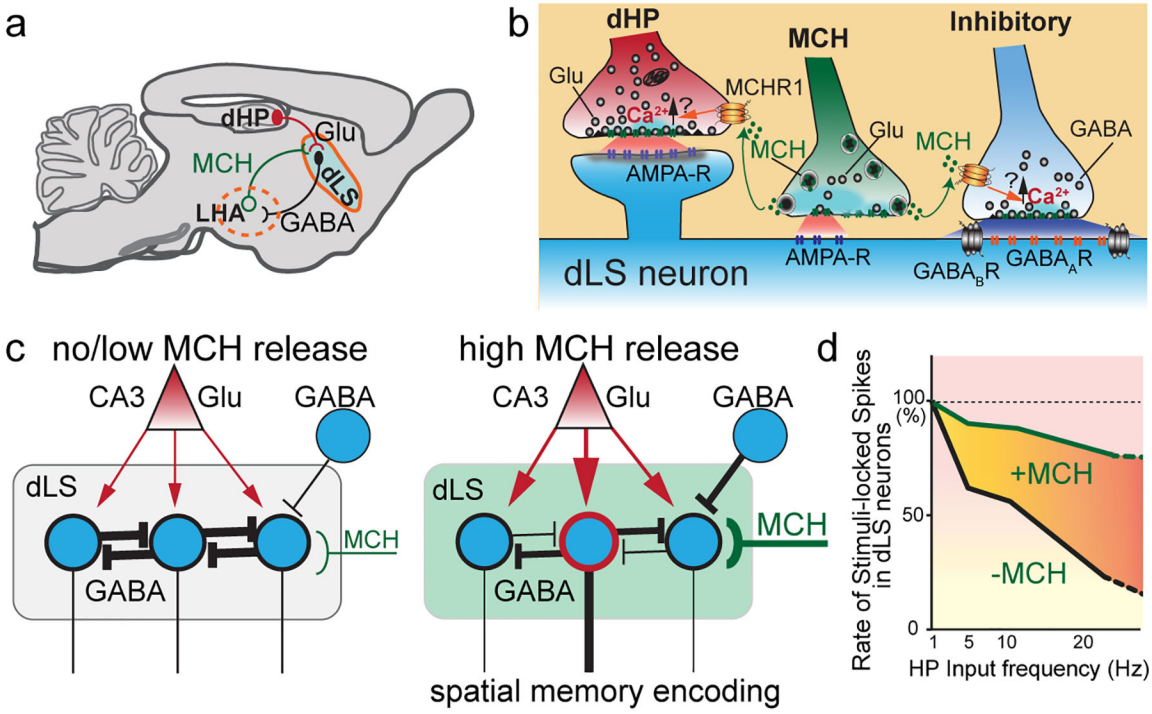

Extended Data Fig. 9. Summary of inferred mechanism through which MCH regulates hippocampo-septal neurocircuits.

a, Diagram of hippocampo-septal circuit, including the role of MCH releasing neurons (green). **b**, Diagram showing presynaptic regulation of both excitatory and inhibitory synaptic inputs onto a dLS neuron. Synaptic release of GABA activates both $GABA_A$ and $GABA_B$ receptors. **c**, Downstream impact of MCH release on dLS neurons. *Left*: in the absence of MCH, strong collateral inhibition limits the hippocampal-dLS excitatory

synaptic inputs induced dLS neuronal firing. *Right:* In the presence of MCH, dLS neurons are silenced by MCH-induced enhancement of GABAergic inhibition. This in turn reduces the collateral inhibition. However, MCH also enhances dHP-dLS excitatory synaptic inputs, thus enabling the postsynaptic dLS neuron to fire in high fidelity with HP neuronal firing. **d**, Plot depicts that MCH enhances dLS neuronal firing fidelity in response to HP inputs and thus increased the dynamic range of firing capacity.

Supplementary Material

Refer to Web version on PubMed Central for supplementary material.

Acknowledgments

We would like to thank Dr György Buzsáki and members of the Tsien laboratory, especially Dr. Xiaohan Wang and Dr. Ethan McCurdy, for their critical reading and constructive suggestions. We would like to thank Drs. Alexander Kusnecov, Chiara Manzini, Baijuan Xia, Audrey Chang, and Yiyao Zhang for their generous help in the behavioral tests and analyses. We also want to thank Drs. Arnold Rabson and Nicola Francis of Rutgers for their input on the manuscript. We especially would like to thank Drs. Brett Mensh, Gabrielle Edgerton and Sandra Aamodt for their critical input and suggestions on the manuscript. We want to thank Drs. Zhuo-Ran Xu, Vivian Li and Jessica Salvatore for suggestions on statistical analyses. The Pang laboratory is supported by NIH R01AA023797, NIH RF1MH120144 and in part by the Robert Wood Johnson Foundation (grant #74260) to the Child Health Institute of New Jersey.

References

1. van den Pol AN Neuropeptide transmission in brain circuits. Neuron 76, 98–115 (2012). [PubMed: 23040809]
2. Bargmann CI & Marder E From the connectome to brain function. Nat Methods 10, 483–490 (2013). [PubMed: 23866325]
3. Marder E Neuromodulation of neuronal circuits: back to the future. Neuron 76, 1–11 (2012). [PubMed: 23040802]
4. Qu D, et al. A role for melanin-concentrating hormone in the central regulation of feeding behaviour. Nature 380, 243–247 (1996). [PubMed: 8637571]
5. Bittencourt JC, et al. The melanin-concentrating hormone system of the rat brain: an immuno- and hybridization histochemical characterization. J Comp Neurol 319, 218–245 (1992). [PubMed: 1522246]
6. Bittencourt JC Anatomical organization of the melanin-concentrating hormone peptide family in the mammalian brain. Gen Comp Endocrinol 172, 185–197 (2011). [PubMed: 21463631]
7. Steininger TL, Kilduff TS, Behan M, Benca RM & Landry CF Comparison of hypocretin/orexin and melanin-concentrating hormone neurons and axonal projections in the embryonic and postnatal rat brain. J Chem Neuroanat 27, 165–181 (2004). [PubMed: 15183202]
8. Jego S, et al. Optogenetic identification of a rapid eye movement sleep modulatory circuit in the hypothalamus. Nat Neurosci 16, 1637–1643 (2013). [PubMed: 24056699]
9. Vetrivelan R, et al. Melanin-concentrating hormone neurons specifically promote rapid eye movement sleep in mice. Neuroscience 336, 102–113 (2016). [PubMed: 27595887]
10. Adamantidis A & de Lecea L A role for Melanin-Concentrating Hormone in learning and memory. Peptides 30, 2066–2070 (2009). [PubMed: 19576257]
11. Blouin AM, et al. Human hypocretin and melanin-concentrating hormone levels are linked to emotion and social interaction. Nat Commun 4, 1547 (2013). [PubMed: 23462990]
12. Whiddon BB & Palmiter RD Ablation of neurons expressing melanin-concentrating hormone (MCH) in adult mice improves glucose tolerance independent of MCH signaling. J Neurosci 33, 2009–2016 (2013). [PubMed: 23365238]

13. Domingos AI, et al. Hypothalamic melanin concentrating hormone neurons communicate the nutrient value of sugar. Elife 2, e01462 (2013). [PubMed: 24381247]
14. Adams AC, et al. Ablation of the hypothalamic neuropeptide melanin concentrating hormone is associated with behavioral abnormalities that reflect impaired olfactory integration. Behav Brain Res 224, 195–200 (2011). [PubMed: 21669232]
15. Kosse C & Burdakov D Natural hypothalamic circuit dynamics underlying object memorization. Nat Commun 10, 2505 (2019). [PubMed: 31175285]
16. Brailoiu GC, et al. Nesfatin-1: distribution and interaction with a G protein-coupled receptor in the rat brain. Endocrinology 148, 5088–5094 (2007). [PubMed: 17627999]
17. Elias CF, et al. Characterization of CART neurons in the rat and human hypothalamus. J Comp Neurol 432, 1–19 (2001). [PubMed: 11241374]
18. Chee MJ, Arrigoni E & Maratos-Flier E Melanin-concentrating hormone neurons release glutamate for feedforward inhibition of the lateral septum. J Neurosci 35, 3644–3651 (2015). [PubMed: 25716862]
19. Izawa S, et al. REM sleep–active MCH neurons are involved in forgetting hippocampus-dependent memories. Science 365, 1308–1313 (2019). [PubMed: 31604241]
20. Pereira-Da-Silva M, De Souza CT, Gasparetti AL, Saad MJA & Velloso LA Melanin-concentrating hormone induces insulin resistance through a mechanism independent of body weight gain. J Endocrinol 186, 193–201 (2005). [PubMed: 16002548]
21. Jeon JY, et al. MCH−/− mice are resistant to aging-associated increases in body weight and insulin resistance. Diabetes 55, 428–434 (2006). [PubMed: 16443777]
22. Adamantidis A, et al. Disrupting the melanin-concentrating hormone receptor 1 in mice leads to cognitive deficits and alterations of NMDA receptor function. Eur J Neurosci 21, 2837–2844 (2005). [PubMed: 15926931]
23. Pachoud B, et al. Major impairments of glutamatergic transmission and long-term synaptic plasticity in the hippocampus of mice lacking the melanin-concentrating hormone receptor-1. J Neurophysiol 104, 1417–1425 (2010). [PubMed: 20592115]
24. Shimada M, Tritos NA, Lowell BB, Flier JS & Maratos-Flier E Mice lacking melanin-concentrating hormone are hypophagic and lean. Nature 396, 670–674 (1998). [PubMed: 9872314]
25. Risold PY & Swanson LW Connections of the rat lateral septal complex. Brain Res Brain Res Rev 24, 115–195 (1997). [PubMed: 9385454]
26. Swanson LW & Cowan WM The connections of the septal region in the rat. J Comp Neurol 186, 621–655 (1979). [PubMed: 15116692]
27. Tingley D & Buzsaki G Transformation of a Spatial Map across the Hippocampal-Lateral Septal Circuit. Neuron 98, 1229–1242 e1225 (2018). [PubMed: 29779942]
28. Zhou TL, Tamura R, Kuriwaki J & Ono T Comparison of medial and lateral septal neuron activity during performance of spatial tasks in rats. Hippocampus 9, 220–234 (1999). [PubMed: 10401638]
29. Gonzalez JA, Iordanidou P, Strom M, Adamantidis A & Burdakov D Awake dynamics and brain-wide direct inputs of hypothalamic MCH and orexin networks. Nat Commun 7, 11395 (2016). [PubMed: 27102565]
30. Hassani OK, Lee MG & Jones BE Melanin-concentrating hormone neurons discharge in a reciprocal manner to orexin neurons across the sleep-wake cycle. Proc Natl Acad Sci U S A 106, 2418–2422 (2009). [PubMed: 19188611]
31. Blanco-Centurion C, et al. Dynamic Network Activation of Hypothalamic MCH Neurons in REM Sleep and Exploratory Behavior. J Neurosci 39, 4986–4998 (2019). [PubMed: 31036764]
32. Kong D, et al. Glucose stimulation of hypothalamic MCH neurons involves K(ATP) channels, is modulated by UCP2, and regulates peripheral glucose homeostasis. Cell Metab 12, 545–552 (2010). [PubMed: 21035764]
33. Phelan KD, Hasuo H, Twery MJ & Gallagher JP Projection neurons in the rat dorsolateral septal nucleus possess recurrent axon collaterals. Neurosci Lett 97, 259–265 (1989). [PubMed: 2469995]
34. Arrigoni E & Saper CB What optogenetic stimulation is telling us (and failing to tell us) about fast neurotransmitters and neuromodulators in brain circuits for wake-sleep regulation. Curr Opin Neurobiol 29, 165–171 (2014). [PubMed: 25064179]

35. Park JY, et al. Novel Neuroprotective Effects of Melanin-Concentrating Hormone in Parkinson's Disease. Mol Neurobiol 54, 7706–7721 (2017). [PubMed: 27844281]
36. Tan CP, et al. Melanin-concentrating hormone receptor subtypes 1 and 2: species-specific gene expression. Genomics 79, 785–792 (2002). [PubMed: 12036292]
37. Saito Y, et al. Molecular characterization of the melanin-concentrating-hormone receptor. Nature 400, 265–269 (1999). [PubMed: 10421368]
38. Chee MJ, Pissios P & Maratos-Flier E Neurochemical characterization of neurons expressing melanin-concentrating hormone receptor 1 in the mouse hypothalamus. J Comp Neurol 521, 2208–2234 (2013). [PubMed: 23605441]
39. Kokkotou EG, Tritos NA, Mastaitis JW, Slieker L & Maratos-Flier E Melanin-concentrating hormone receptor is a target of leptin action in the mouse brain. Endocrinology 142, 680–686 (2001). [PubMed: 11159839]
40. Engle SE, et al. A CreER mouse to study melanin concentrating hormone signaling in the developing brain. Genesis 56, e23217 (2018). [PubMed: 29806135]
41. David DJ, et al. Efficacy of the MCHR1 antagonist N-[3-(1-{[4-(3,4-difluorophenoxy)phenyl]methyl}(4-piperidyl))-4-methylphenyl]-2-m ethylpropanamide (SNAP 94847) in mouse models of anxiety and depression following acute and chronic administration is independent of hippocampal neurogenesis. J Pharmacol Exp Ther 321, 237–248 (2007). [PubMed: 17237257]
42. Owen SF, Liu MH & Kreitzer AC Thermal constraints on in vivo optogenetic manipulations. Nat Neurosci 22, 1061–1065 (2019). [PubMed: 31209378]
43. Margeta-Mitrovic M, Mitrovic I, Riley RC, Jan LY & Basbaum AI Immunohistochemical localization of GABA(B) receptors in the rat central nervous system. J Comp Neurol 405, 299–321 (1999). [PubMed: 10076927]
44. O'Keefe J & Dostrovsky J The hippocampus as a spatial map. Preliminary evidence from unit activity in the freely-moving rat. Brain Res 34, 171–175 (1971). [PubMed: 5124915]
45. Huxter J, Burgess N & O'Keefe J Independent rate and temporal coding in hippocampal pyramidal cells. Nature 425, 828–832 (2003). [PubMed: 14574410]
46. O'Keefe J & Recce ML Phase relationship between hippocampal place units and the EEG theta rhythm. Hippocampus 3, 317–330 (1993). [PubMed: 8353611]
47. Ranck JB Jr. Studies on single neurons in dorsal hippocampal formation and septum in unrestrained rats. I. Behavioral correlates and firing repertoires. Exp Neurol 41, 461–531 (1973). [PubMed: 4355646]
48. Kjelstrup KB, et al. Finite scale of spatial representation in the hippocampus. Science 321, 140–143 (2008). [PubMed: 18599792]
49. Takamura Y, et al. Spatial firing properties of lateral septal neurons. Hippocampus 16, 635–644 (2006). [PubMed: 16786557]
50. Conejo NM, Gonzalez-Pardo H, Gonzalez-Lima F & Arias JL Spatial learning of the water maze: progression of brain circuits mapped with cytochrome oxidase histochemistry. Neurobiol Learn Mem 93, 362–371 (2010). [PubMed: 19969098]
51. Leroy F, et al. A circuit from hippocampal CA2 to lateral septum disinhibits social aggression. Nature 564, 213–218 (2018). [PubMed: 30518859]
52. Antonawich FJ, Melton CS, Wu P & Davis JN Nesting and shredding behavior as an indicator of hippocampal ischemic damage. Brain Res 764, 249–252 (1997). [PubMed: 9295218]
53. Armbruster BN, Li X, Pausch MH, Herlitze S & Roth BL Evolving the lock to fit the key to create a family of G protein-coupled receptors potently activated by an inert ligand. Proc Natl Acad Sci U S A 104, 5163–5168 (2007). [PubMed: 17360345]
54. Schneeberger M, et al. Functional analysis reveals differential effects of glutamate and MCH neuropeptide in MCH neurons. Mol Metab 13, 83–89 (2018). [PubMed: 29843980]
55. Ferrante M, Migliore M & Ascoli GA Feed-forward inhibition as a buffer of the neuronal input-output relation. P Natl Acad Sci USA 106, 18004–18009 (2009).
56. Gao XB Electrophysiological effects of MCH on neurons in the hypothalamus. Peptides 30, 2025–2030 (2009). [PubMed: 19463877]

57. Saito Y, Cheng M, Leslie FM & Civelli O Expression of the melanin-concentrating hormone (MCH) receptor mRNA in the rat brain. J Comp Neurol 435, 26–40 (2001). [PubMed: 11370009]

58. Tingley D & Buzsaki G Routing of Hippocampal Ripples to Subcortical Structures via the Lateral Septum. Neuron 105, 138–149 e135 (2020). [PubMed: 31784288]

59. Rawlins JN & Olton DS The septo-hippocampal system and cognitive mapping. Behav Brain Res 5, 331–358 (1982). [PubMed: 7126316]

60. Manning JR, Jacobs J, Fried I & Kahana MJ Broadband shifts in local field potential power spectra are correlated with single-neuron spiking in humans. J Neurosci 29, 13613–13620 (2009). [PubMed: 19864573]

61. Liu JJ, Bello NT & Pang ZP Presynaptic Regulation of Leptin in a Defined Lateral Hypothalamus-Ventral Tegmental Area Neurocircuitry Depends on Energy State. J Neurosci 37, 11854–11866 (2017). [PubMed: 29089444]

62. Vogel-Ciernia A & Wood MA Examining object location and object recognition memory in mice. Curr Protoc Neurosci 69, 8 31 31–17 (2014). [PubMed: 25297693]

63. Glass R, Norton S, Fox N & Kusnecov AW Maternal immune activation with staphylococcal enterotoxin A produces unique behavioral changes in C57BL/6 mouse offspring. Brain Behav Immun 75, 12–25 (2019). [PubMed: 29772261]

64. Vorhees CV & Williams MT Morris water maze: procedures for assessing spatial and related forms of learning and memory. Nat Protoc 1, 848–858 (2006). [PubMed: 17406317]

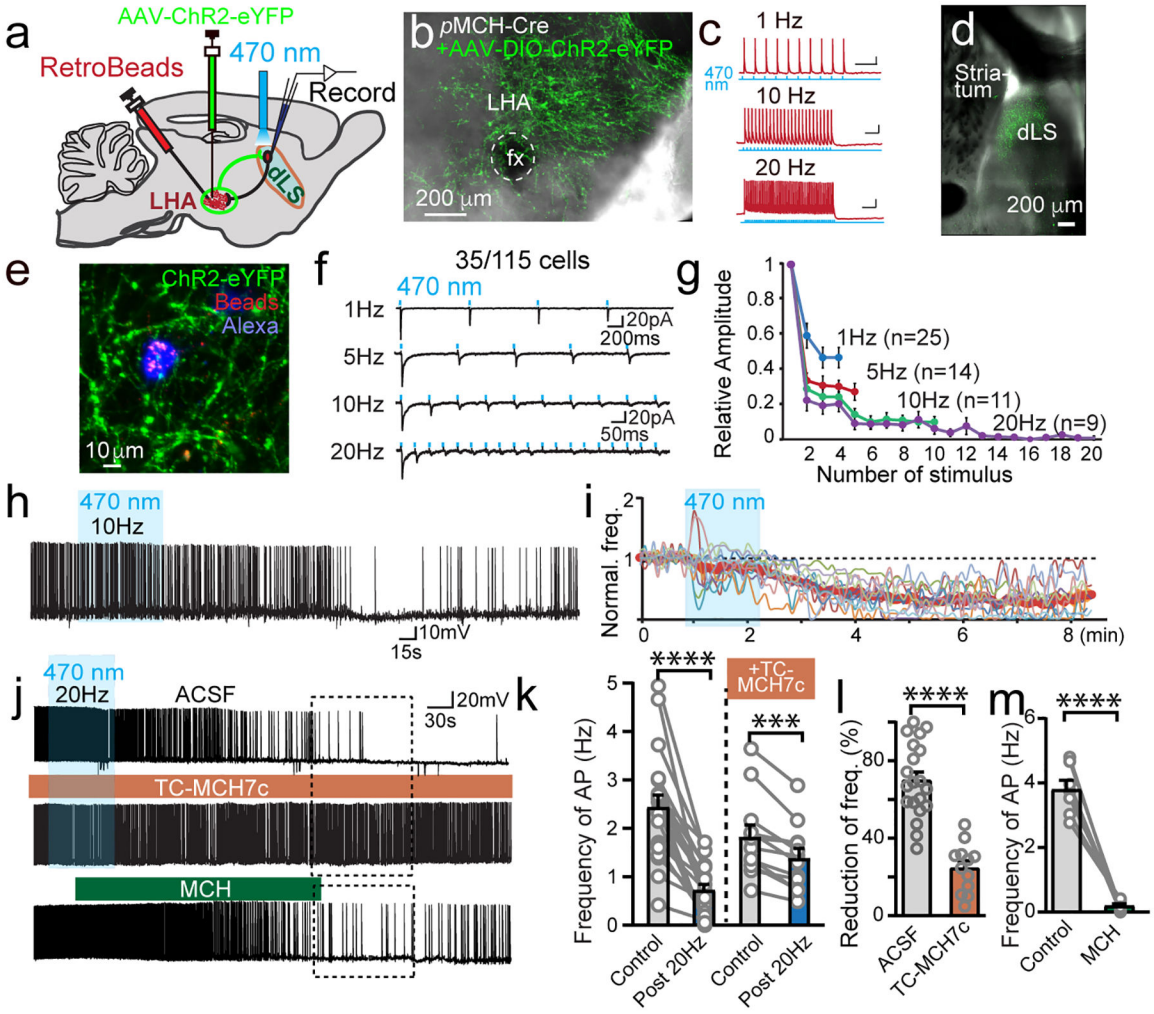

Fig.1 |. Endogenous MCH suppresses spontaneous neural activity in the dLS.

a, Diagram of the experimental setup. Retrograde fluorescent microbeads and AAV-DIO-ChR2 were sequentially injected into the LHA of MCH-Cre mice. Retro-labeled dLS neurons were analyzed by whole cell patch clamp recording. **b**, Representative image of MCH-expressing neurons expressing Cre-dependent ChR2-eYFP. **c**, LHA MCH-expressing neurons can be reliably evoked to fire action potentials up to 20Hz following optogenetic activation. **d**, ChR2-eYFP positive axonal projections from MCH neurons were identified in the dLS. **e**, An example of a Retrobead-labeled dLS-to-LHA projecting neuron that was recorded and loaded with Alexa Fluor 633 dye and surrounding MCH fibers. **f**, Sample traces of MCH neuronal axonal optogenetic stimulation-induced oEPSCs in dLS-to-LHA projecting neurons. 35 out of 115 cells showed oEPSCs. **g**, Pooled data showing oEPSCs of MCH neuron origin depressed quickly. **h**, Sample trace showing that spontaneous action potential firing (sAP) of dLS neurons was suppressed by prolonged light stimulation (10Hz for 80s) on ChR-expressing MCH axons. **i**, Normalized frequency of sAPs in dLS-to-LHA projecting neurons. The thick red line shows the average frequency over time. **j**, Sample traces of sAPs under different conditions; **k**, Pooled data showing the changes of sAPs with or without MCHR-1 blocker. n=20 /8 and 12/4, neurons/mice, in ACSF or in the presence

of TC-MCH7c, respectively. Data are mean ± SEM. Paired two-tailed Student's t-tests were used, p<0.0001 in ACSF, p=0.0002 in Tc MCH7c. **l**, Percentage of reduction of frequency after 20Hz optogenetic stimulation of MCH neuronal fibers in the dLS in ACSF (n=20/8, neurons/mice) or in the presence of MCHR1 blocker TC-MCH7c (n=12/4, neurons/mice). Data are mean ± SEM. Unpaired two-tailed Student's t-tests were used, p<0.0001. **m**, Pooled data showing the frequency of sAPs after the application of MCH (600 nM), n=7/3, neurons/mice. Paired two-tailed Student's t-tests were used. p<0.0001. Data are mean ± SEM. ***p<0.001, ****p<0.0001

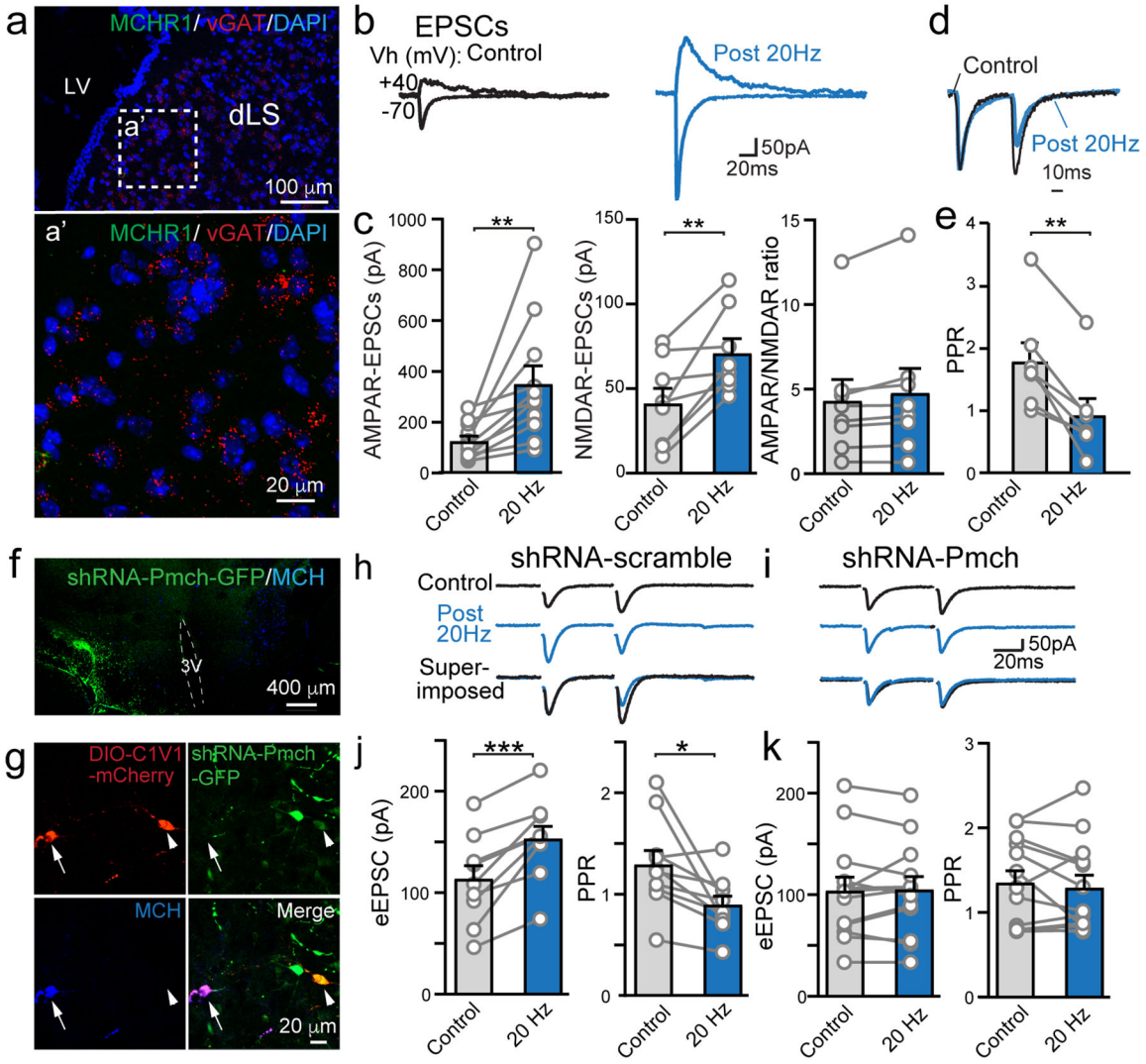

Fig.2 |. MCH enhances excitatory synaptic transmission in the HP-to-dLS pathway.

a, RNAscope *in situ* hybridization result using probes against MCHR1 and vGAT. **b**, Sample traces of evoked AMPAR- (Vh=−70 mV) and NMDAR- (Vh=+40 mV) mediated EPSCs in dLS-LHA neurons via field stimulations before (control) and after 20Hz 2min optogenetic stimulation of MCH axons expressing ChR2. **c**, Pooled normalized data showing the amplitude of AMPAR-EPSCs (n=11/8, neurons/mice), NMDAR-EPSCs (n=8/6, neurons/mice), and ratios of AMPAR-EPSC/NMDAR-EPSC (n=8/6, neurons/mice). Numbers of neurons/animals analyzed are indicated in bars. Paired two-tailed Student's t-tests were used, AMPAR-EPSC, p=0.0057; NMDAR-EPSC, p=0.0064; and AMPAR/NMDAR ratio, p=0.0508. **d**, Superimposed sample traces of evoked EPSCs by paired pulses of field stimulations pre- and post-prolonged optogenetic stimulation. **e**, Pooled data of paired-pulse ratio (PPR) and the normalized amplitudes of evoked EPSCs (n=7/6, neurons/mice). Paired two-tailed Student's t-tests were used, p=0.0014. **f**, shRNA knockdown of Pmch in the hypothalamus in MCH-Cre mice. Viruses were injected into one side. **g**, AAV-DIO-C1V1 injection-labeled MCH neurons (arrow and arrowhead). shRNA-infected neurons show no

expression of MCH (arrowhead). **h**, Representative evoked EPSCs and pooled data in control (shRNA-scramble). **i**, Representative evoked EPSCs in MCH knockdown (shRNA-Pmch) animals. **j**, Pooled data of evoked EPSCs and PPR in scramble shRNA group, n=9/4, neurons/animals; Paired two-tailed Student's t-tests were used. p=0.004 for eEPSC and p=0.016 for PPR. **k**. Pooled data of evoked EPSCs and paired-pulse ratio in shRNA-Pmch group, n=12/3, neurons/animals. Paired two-tailed Student's t-tests were used, p=0.774 for eEPSCs, and p=0.4796 for PPR. Data are mean ± SEM. *p<0.05, **p<0.01, ***p<0.001, ****p<0.0001.

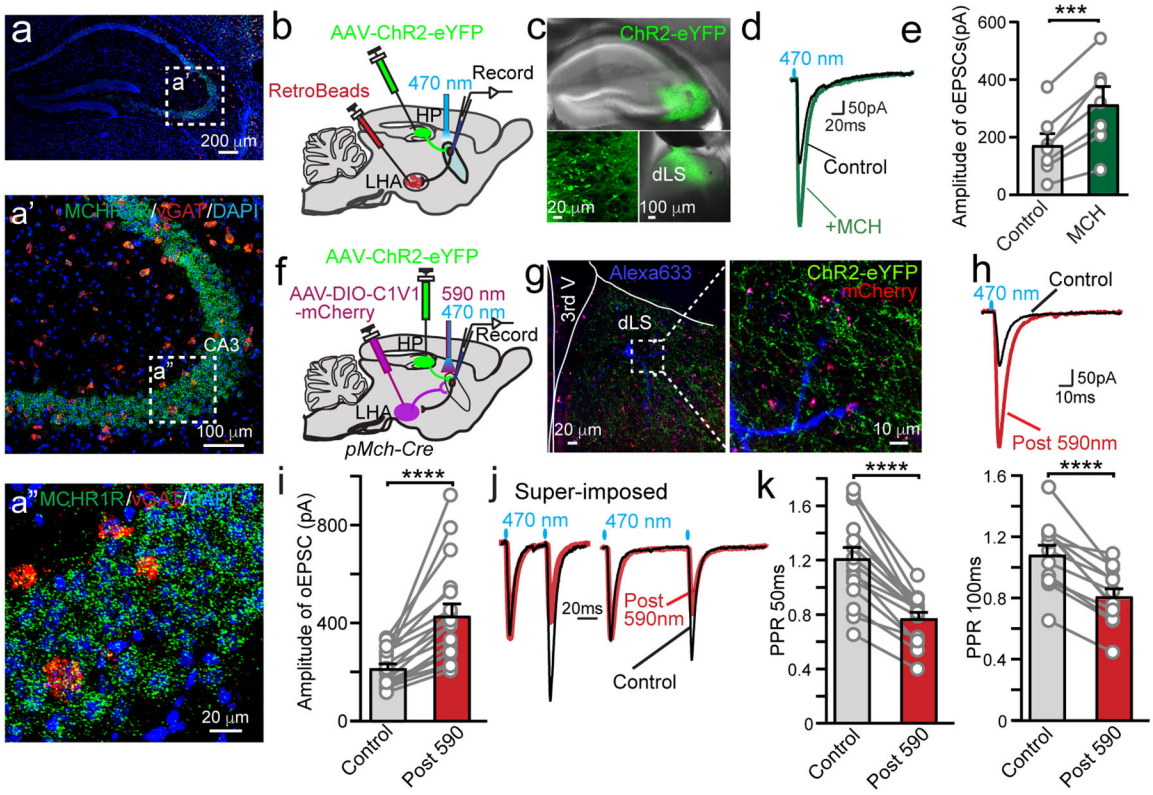

Fig.3 |. MCH enhances excitatory synaptic transmission in the dHP-to-dLS pathway.

a, Representative images from RNAScope *in situ* hybridization showing the expression of MCHR1 and vGAT in the dHP. **b**, Diagram of experiments probing functional connections in the hippocampo-septo-LHA pathway. RetroBeads were injected into the LHA while AAV-ChR2-eYFP was injected into the ventral HP. Retro-labeled dLS-LHA neurons were analyzed by whole cell patch clamp recording. **c**, Viral-mediated expression of ChR2-eYFP in CA3 neurons. *Insets* show CA3 neurons expressing ChR2-eYFP and ChR2-eYFP-labeled axonal projections in the dLS. **d**, Sample traces of optogenetically-stimulated EPSCs (oEPSCs) recorded from dLS-LHA neurons, pre- (black trace) and post- (green trace) bath application of MCHR agonist MCH (600nM). **e**, Pooled oEPSCs data, n=7/3, neurons/mice. Paired two-tailed Student's t-tests were used, p=0.0008. **f**, Diagram of experimental setup for dual optogenetic stimulations (470 nm and 590 nm) to determine HP origin of oEPSCs (ChR2) and MCH neuronal origin of endogenous MCH release (red shifted C1V1), respectively. AAV-ChR2-eYFP was injected into the dHP and AAV-DIO-C1V1-mCherry was injected into the LHA of MCH-Cre mice. dLS neurons were analyzed by whole cell recording. **g**, Viral-mediated expression of C1V1-mCherry in MCH neurons and ChR2-eYFP in hippocampal CA3 neurons. Infected neuronal fibers from the HP (eYFP+) and MCH neurons (mCherry+) with the recorded neuron loaded with Alexa633 in the dLS region. **h**, Optogenetics-induced oEPSCs in the dLS pre- and post-prolonged 590nm light activation of C1V1-positive MCH axons. **i**, Pooled single oEPSC amplitude data. n=18/5, neurons/mice. Paired two-tailed Student's t-tests were used, p<0.0001. **j**, Sample traces of oEPSCs after paired-pulse optogenetic stimulation. **k**, Pooled data of PPRs of oEPSCs at stimulation intervals of 50 ms (n=16/5, neurons/mice) and 100 ms (n=13/5, neurons/mice).

Paired two-tailed Student's t-tests were used, $p<0.0001$ in both plots. Data are mean ± SEM; Paired two-tailed Student's t-tests were used: ***$p<0.001$, ****$p<0.0001$.

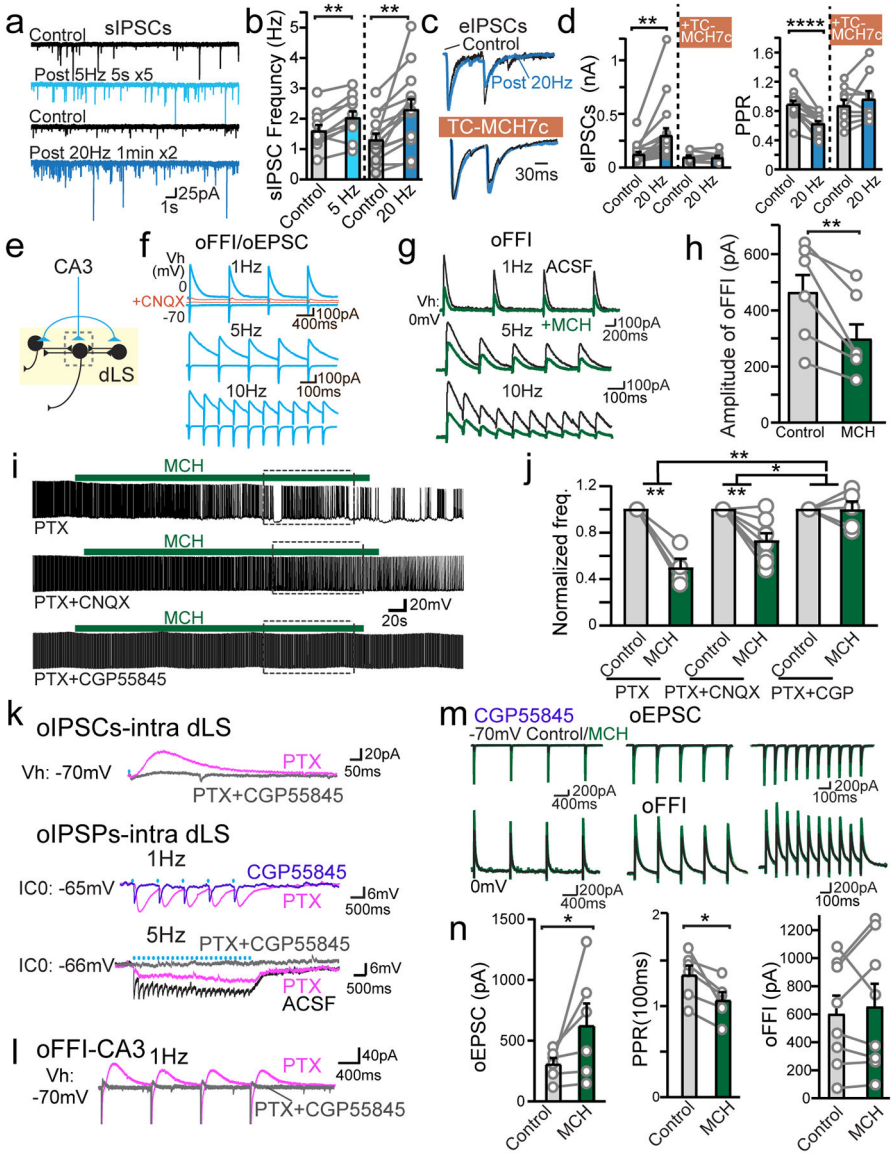

Fig. 4 |. Augmentation of inhibitory synaptic transmission by MCH accounts for the suppressive effect on dLS neuronal activity and excitability.

a, Sample traces of spontaneous IPSCs (sIPSCs) mediated by $GABA_A$ receptor ($GABA_AR$) in dLS neurons projecting to the LHA, pre- and post-20Hz, 2min optogenetic stimulation of ChR-positive MCH axons. AMPAR blocker CNQX and NMDAR blocker AP5 were present in the bath to isolate inhibitory transmission. **b**, Pooled sIPSC data showing facilitation after 5 Hz (n=11/9, neurons/mice) and 20 Hz (n=14/9, neurons/mice) optogenetic stimulation. Paired two-tailed Student's t-tests were used, p=0.0015 (5Hz) and p=0.0017 (20Hz). **c**, Superimposed sample traces of evoked IPSCs with paired pulses of field stimulations (eIPSCs) pre- and post- optogenetic stimulation, with or without MCHR antagonist TC-MCH7c in bath. **d**, Pooled data of normalized amplitudes of eIPSCs (left) and PPRs (right) with (n=9/6, neurons/mice) or without (n=17/10, neurons/mice) MCHR antagonist TC-MCH7c in bath. Amplitude: p=0.0028 (control) and p=0.7379 (Tc-MCH7c); PPR: p<0.0001 (control) and p=0.2778 (Tc-MCH7c). **e**, Diagram of HP input-induced oEPSC

and feed-forward inhibition (oFFI). AAV-ChR2-eYFP was injected into the dorsal CA3. **f**, Sample traces of HP-origin oEPSC and secondary oFFI in dLS neurons at varied frequencies. Both components were blocked by CNQX. **g**, Sample traces of hippocampal oFFI pre- (black) or post-MCH (green). **h**, Pooled oFFI amplitude data. n=6/3, neurons/mice. Paired two-tailed Student's t-tests were used. p=0.0034. **i**, Sample traces showing the impacts of MCH over sAP of dLS neurons during the blockage of $GABA_AR$, $GABA_AR$ and AMPAR, or $GABA_AR$ and $GABA_BR$. **j**, Pooled data. n=4/3, 8/4, 5/3, neurons/mice, in PTX, PTX+CNQX and PTX+CGP groups. 2-way ANOVA, $F(2,14)=9.125$, p=0.0029. *Posthoc* turkey test was used for multiple comparison between groups: PTX vs. PTX+CGP **p=0.002; PTX+CNQX vs PTX+CGP *p=0.045. **k**, Sample traces of the sum and isolation of both $GABA_AR$- and $GABA_BR$-mediated components in collateral oIPSCs and oIPSPs. **l**, Sample traces of the hippocampal oEPSC and $GABA_BR$-mediated oFFI-IPSC. **m**, Sample traces of primary HP-origin oEPSC and secondary oFFI in dLS neurons in the presence of $GABA_BR$ antagonist CGP55845 at varied frequencies pre (black traces) or post MCH (green traces). **n**, Pooled data showing the amplitudes of oEPSCs (n=6/3, neurons/mice), PPR (n=6/3, neurons/mice), and oFFIs in the presence of CGP55845 (n=8/3, neurons/mice). Data are mean ± SEM; numbers of neurons/animals analyzed are indicated in bars. Paired two-tailed Student's t-tests were used, p=0.0491 (oEPSC); p=0.0161 (PPR); p=0.5431 (oFFI). * $p<0.05$, ** $p<0.01$, *** $p<0.0001$.

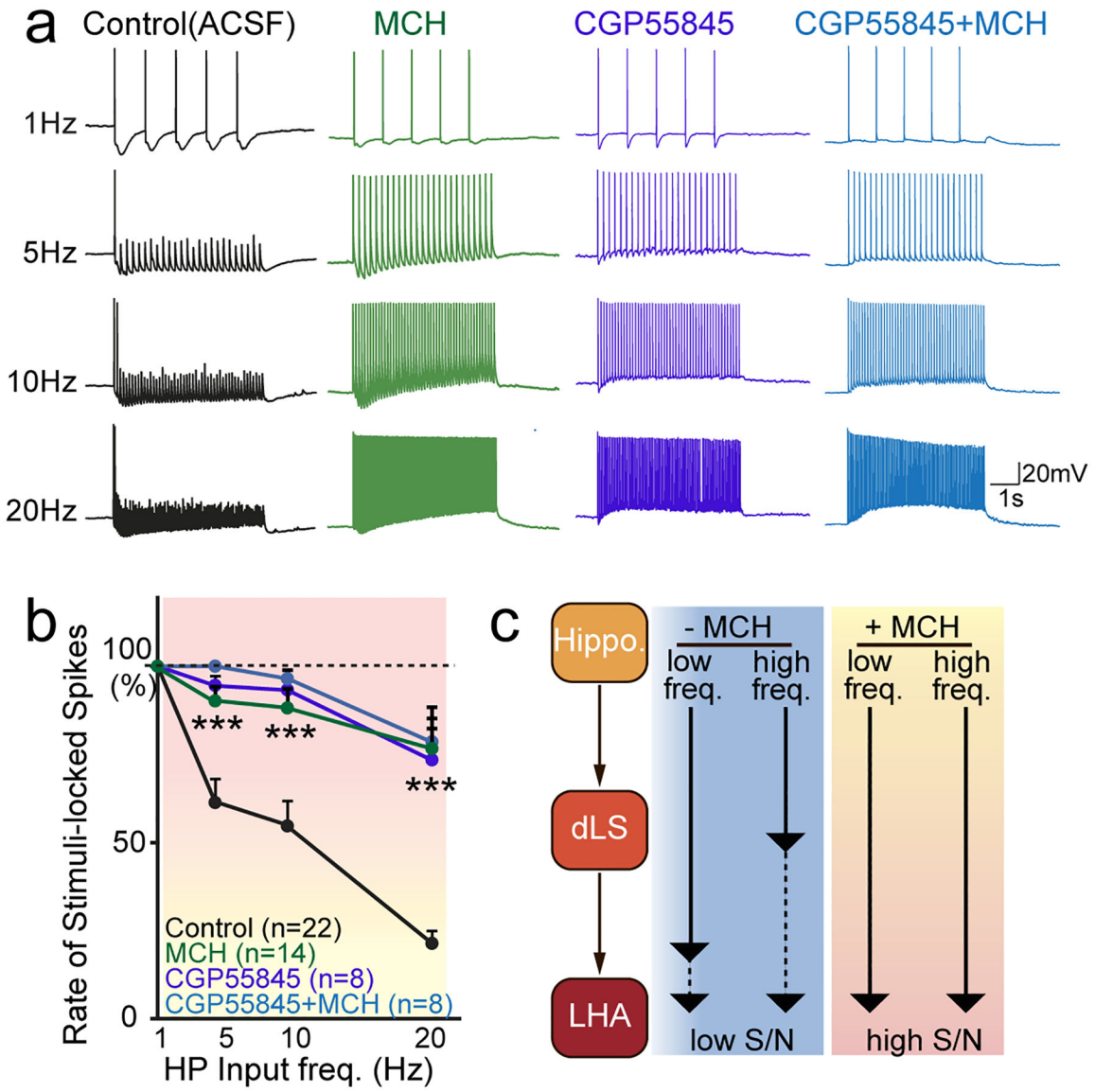

Fig. 5 |. MCH enables high-frequency-coded information flow in the HP-dLS-LHA circuit.

a, Sample traces of oAPs in dLS-to-LHA projecting neurons under different conditions, as labeled. **b**, Pooled data of the ratio of oAPs of dLS neurons as a function of the frequency of hippocampal optogenetic stimulations. **c**, Model of permissive effects of MCH on spike coupling between hippocampal inputs and dLS neuron firing. Two-Way ANOVA tests were used, $F(9,192)$, $P<0.0001$; *Posthoc* Tukey's multiple comparisons, Control vs. MCH $p<0.001$; Control vs. CGP55845 $p<0.001$; Control vs. CGP+MCH $p<0.001$. All data are presented as mean ± SEM. *$p<0.05$, **$p<0.01$, ***$p<0.001$, ****$p<0.0001$.

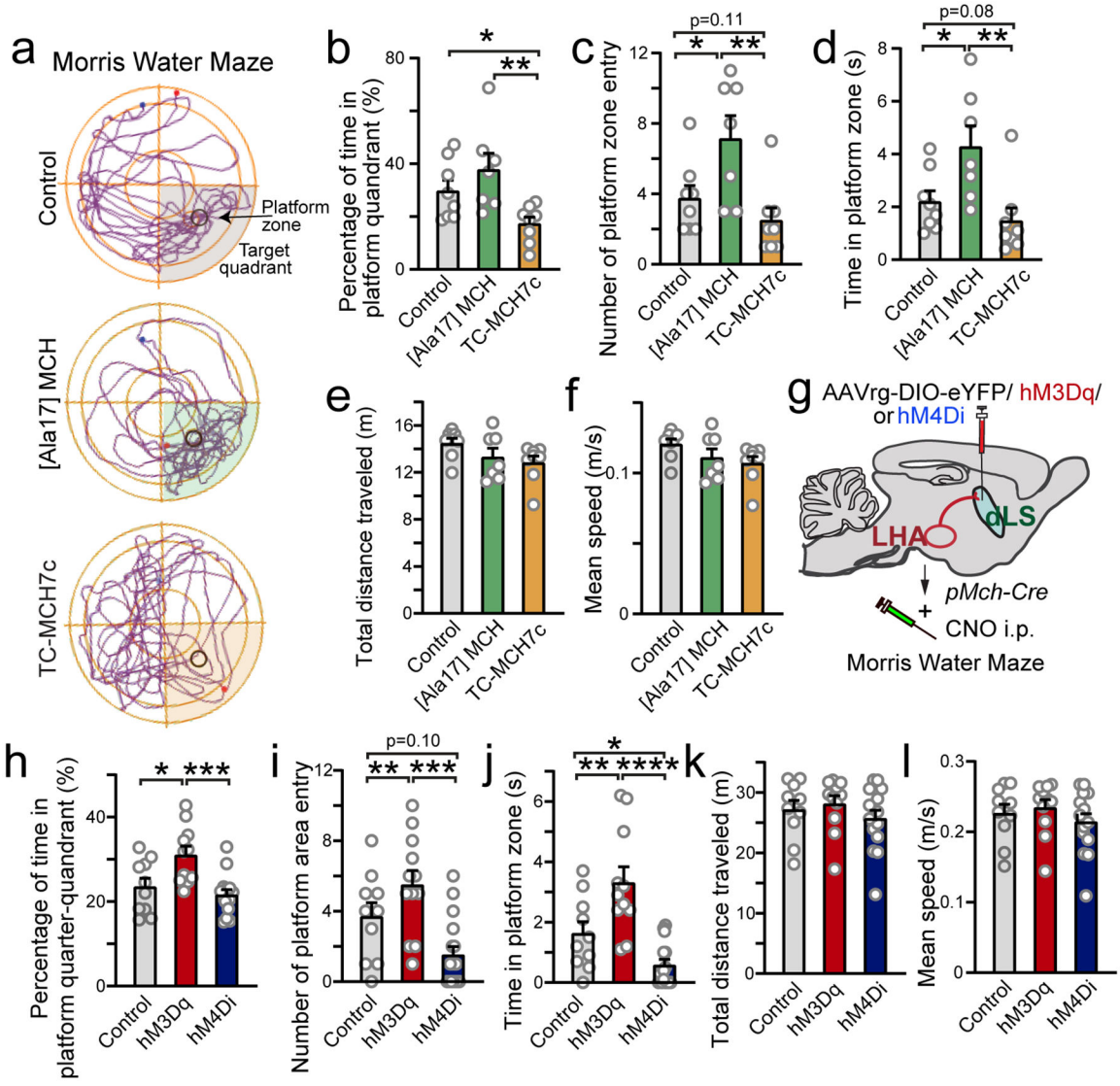

Fig. 6 |. MCH is required for HP-dependent spatial learning and memory consolidation.

a, Representative travel paths of animals in Morris Water Maze test. Animals were locally infused (bilateral cannula targeting the dLS) with vehicle (phosphate-buffered saline), MCHR agonist [Ala17]-MCH, or the MCHR antagonist TC-MCH7c. **b**, Percentage of time in platform quadrant. Non-parametric Kruskal-Wallis one-way ANOVA, p=0.01104; *posthoc* Mann Whitney test, Control vs. MCH p=0.2472; Control vs. TC-MCH7c p=0.05; MCH vs. TC-MCH7c p=0.0038. **c**, Number of target zone head entries. Non-parametric Kruskal-Wallis one-way ANOVA, p=0.0063; *posthoc* Mann Whitney test, Control vs. MCH p=0.0349; Control vs. TC-MCH7c p=0.1074; MCH vs. TC-MCH7c p=0.0069. **d**, Time of head spending in the target zone. Non-parametric Kruskal-Wallis one-way ANOVA, p=0.007744; *posthoc* Mann Whitney test, Control vs. MCH p=0.036; Control vs. TC-MCH7c p=0.08; MCH vs. TC-MCH7c p=0.0065.. **e**, Pooled data of the total distance traveled. Non-parametric Kruskal-Wallis one-way ANOVA, p=0.1039. **f**, Mean speed. Non-parametric Kruskal-Wallis one-way ANOVA, p=0.1117. **a-f**, n=8,7,8 in control, MCH

and TC-MCH7c groups, respectively. **g, g**, Diagram showing the retrograde chemogenetic manipulation of LH-to-dLS MCH projections. **h**, Percentage of time in target quadrant. Non-parametric Kruskal-Wallis one-way ANOVA, p=0.003187, *posthoc* Mann Whitney test, Control vs. hM3D p=0.0122; Control vs. hM4D p=0.43; hM3D vs. hM4D p=0.0009. **i**, Number of platform area head entries. Non-parametric Kruskal-Wallis one-way ANOVA, $p=3.939\times10^{-4}$, *posthoc* Mann Whitney test, Control vs. hM3D p=0.00932; Control vs. hM4D p=0.10016; hM3D vs. hM4D p=0.0021. **j**, Time of head in target zone. Non-parametric Kruskal-Wallis one-way ANOVA, $p=6.327\times10^{-5}$, *posthoc* Mann Whitney test. Control vs. hM3D p=0.0048; Control vs. hM4D p=0.0213; hM3D vs. hM4D $p=6.9\times10^{-5}$. **k**, Pooled data of the total distance traveled. Non-parametric Kruskal-Wallis one-way ANOVA, p=0.3991**. l**, Pooled data of mean speed. Non-parametric Kruskal-Wallis one-way ANOVA, p=0.3794**. h-l**, n=10, 11 and 15, in control, hM3Dq and hM4Di groups, respectively. All data are presented as mean ± SEM. *p<0.05, **p<0.01, ***p<0.001, ****p<0.0001.